CHAPTER 8

94320-M Descriptive Physical Oceanography

David Salmon, Principal Investigator

Prince William Sound Science Center

Cordova, Alaska

April 15, 1995

1994 Final Report

Descriptive Physical Oceanography of Prince William Sound and the Gulf of Alaska

Exxon Valdez Trustee Council Project 94320-M

March 1995

David K. Salmon, James M. Murphy, Shelton M. Gay, Thea M. Thomas

Prince William Sound Science Center
PO Box 705 Cordova, AK 99574

1

Executive Summary

This report is a summary of work completed to date in the physical oceanographic component of the SEA program (94320-M). Many of our initial scientific results are succinctly summarized in the abstract of one of the manuscripts that we have prepared from the 1994 field data collection. The first manuscript deals with the large scale descriptive physical oceanography of Prince William Sound (PWS) and the adjacent Gulf of Alaska (GOA). This manuscript has been submitted for publication in a peer reviewed journal, The Global Atmosphere and Ocean System. We did not include the manuscript, on the advice of several peers, to avoid any potential conflicts with publication in the gray versus peer reviewed literature. We briefly describe in this report a few highlights of the numerous results presented in that paper. About 90% of our analytical work this past winter has been aimed at formulating and resolving problems related to the large scale distributions of physical properties and ocean currents. Since we did not include the full manuscript, and the length of this report has been limited, the results presented here do not accurately reflect the amount of analytical work that has been accomplished within the physical oceanography program. Because of constraints on the length of this report requested of by Dr. Spies, EVOS Chief Scientist, and Dr. Cooney, SEA Lead Scientist, we have not presented here the hundreds of figures and images we have prepared and utilized in our analysis and visualization of the data sets, as is classically done in final reports. These very substantial collections of information are housed at the PWS Science Center. The abstract from a second manuscript is also included. It has not yet been submitted for publication, and is therefore still in a data report format. This work represents about 10% of our analytical efforts for the past winter. The manuscript presents more regional small scale descriptions of physical property distributions in PWS. A substantially modified version of this manuscript will be submitted to the journal Estuaries later in 1995. In addition we have several other manuscripts in preparation that reflect to varying degrees the beginnings of attempts to synthesize biological, geochemical and physical oceanographic data sets.

During 1994, we collected and processed conductivity/temperature/depth (CTD) data from approximately 950 locations in PWS and the GOA. Much of the data was collected during five cruises between April and September of 1994. The data also include a collection of 4 year long time series begun under the Cooperative Fisheries Oceanographic Study (CFOS) program. We have continued to compile the long time series started during CFOS, and plan on continuing data collection at several stations in PWS on a regular basis, contingent upon adequate vessel support during winter. We are working cooperatively with the Alaska Department of Fish and Game on this aspect of the program. We have also examined a substantial subset of our acoustic doppler current profiler (ADCP) data. We are preparing an additional manuscript that focuses exclusively on circulation within PWS from direct ADCP measurements and computed velocity estimates from CTD data.

We are integrating our physical data with other data sets collected during the 1994 SEA field season. In particular, we are examining temporal changes in the vertical distribution of zooplankton at stations SEA 22 (the deepest region in PWS) and SEA 4, both of which were occupied numerous times during 1994. We are examining zooplankton distributions in relation to

FINITE ELEMENT METHODS FOR A PREDATOR-PREY MODEL

Ricap o H. Nochetto

Finite element methods are proposed to investigate a predator-prey model in oceanography, which consists of a bioenergetics model for growth coupled with a model for the dispersion of each population and the manner they coexist and interact. The numerical schemes are designed to cope with special features of the resulting system of coupled nonlinear PDEs for density and ODEs for size. The ultimate goal of this research is estimation and prediction of fish production, a fundamental issue in fish ecology, which will require parameter identification and validation of numerical simulations with experimental data. This is part of an ongoing project with C. Berenstein and V. Patrick, both at the Institute for Systems Research.

1. Model. We describe a model for fish movement and spacial distribution that incorporates movement in response to current local conditions. This is an adaptation of the Keller-Segal model for bacteria chemotaxis [4,p.442], and consists of PDEs like

$$(1) \qquad \frac{\partial u}{\partial t} - \text{div} \, (D \, \text{grad} u + \chi \, u \, \text{grad} \lambda) + f = 0 \qquad \text{in } \Omega$$

for density u, where Ω is a bounded domain in $\mathbf{R}^d$ with $d = 1, 2, 3$; $D, \chi > 0$ are constants. The first term in the divergence corresponds to dispersal by diffusive-like random motions. The second term in the divergence is an advection term describing directed motions with a drift velocity given by the gradient of the so-called *taxis function* λ. Function f is a reaction term describing mortality and regeneration. The typical boundary condition is that of vanishing flux, but other alternatives will be considered.

The role of λ is to characterize the net directed motion at $(\mathbf{x}, t)$ towards more desirable conditions in response to density u and size s at $(\mathbf{x}, t)$ of interacting populations. It can be extended to include migration and bounds on the tolerance of environmental variables (e.g. temperature, salinity, concentrations of nitrogen, phosphorus, dissolved oxygen and light intensity). Considering first the local process, λ is of the form $\lambda = \lambda^*(\varphi^*, \nu^*)$, where φ^* and ν^* are the foraging and encounter model functions that depend on densities, sizes, and environmental variables, and λ^* is the *loss function*. A particular form used in [11] for λ in the case of one active species reads

$$(2) \qquad \lambda^*(\varphi^*, \nu^*) = a(\varphi^* - \varphi_{\max})^2 + b(\nu^*)^2,$$

where a, b are constants and $\varphi_{\max}$, a function of size s, is the supremum of all feeding rates for an individual size s. We may consider more than one predator and prey, in which case (1) becomes a system of PDEs. We may also incorporate size for each population via ODEs with a nonlocal coupling with (1).

An important issue to be faced in this investigation is the formation of narrow transition layers where the solution exhibits a large gradient. This is re ted to the size of $\varepsilon := D/\chi$, which dictates the type of numerical methods to be used: (1) is parabolic for moderate ε but becomes advection-dominated for small ε. Studying the asymptotic behavior of (1) as $\varepsilon \to 0$ is also an integral part of this proposal, more notably when u is vector-valued. Asymptotic limits as $a/b \to 0, \infty$ are also to be examined. Determining layer thickness and profile of u as a function of ε, together with simplified equations dictated by formal asymptotics, is essential in understanding the structure of (1) and being able to exploit it numerically. We refer to [10] for similar issues in the context of hyperbolic systems of conservation laws. Parameter identification (e.g. D, χ, a, b) and its interplay with numerical simulations and data collection and processing is another relevant topic to be considered. The proposed model (2) for λ^* will have to be reeexamined, and possibly adjusted accordingly. Asymptotics may play a role in this process.

2. Numerical Issues. Finite element methods offer a great deal of flexibility in terms of domain approximation, mesh generation, and adaptivity, as opposed to finite differences. We focus the discussion

on a single equation. We do not consider extensions to systems of PDEs at this early stage, but stress that difficulties are expected whenever diffusion and advective-dominated modes occur simultaneously.

The design of a numerical scheme for (1) over a decomposition T of Ω not oriented with the flow must tackle the following two fundamental problems: (a) be (formally) highly accurate where the solution is smooth and (b) be stable without requiring the size of T to be smaller than ε. The usual Galerkin method, as well as centered differences, fail to meet these criteria. Upwinding techniques are a proper remedy in that they are known to be very effective in eliminating, or at least alleviating, spurious numerical oscillations [8]. We propose the use of two distinct classes of finite element methods never tested before in connection with predator-prey models in oceanography. The first scheme, so-called *exponential fitting*, is a mixed method that was introduced for the numerical simulation of semiconductor devices, for which hyperbolicity ($\varepsilon \ll 1$) seems to be more critical than in the present context [3]. We also discuss a *shock-capturing streamline diffusion* method, which is now a popular tool in computational fluid dynamics for advective flows [6,7,8]. Even though these methods are mathematically sound, there are still a number of issues to be explored. The methods are designed to capture rapid transitions and shocks within a few elements and without over and undershooting. Therefore accuracy in regions of smooth behavior seems to be solely dictated by interpolation, but local error estimates and crosswind smearing effect are only known for the streamline diffusion method without shock capturing correction and not for those discussed below. Graded meshes can in principle be used to resolve layers, but their adaptive design and analysis is subject of current research for convection-dominated diffusion problems [5]. It is hoped that this project will not only produce reliable and efficient software for the study and eventual prediction of predator-prey models, but also shed some light on the aforementioned issues in scientific computation.

3. Exponential Fitting via Mixed Methods. Equation (1) is very reminiscent of the evolution equation for charges in semiconductor device modeling. In such a setting $\chi \mathbf{grad}\lambda$ is the electric field and may exhibit, as the taxis function gradient, large amplitudes in relatively small parts of the domain. The Scharfetter-Gummel scheme is very popular to handle the resulting advection-dominated PDE in 1D. Among the various attempts to generalize this method to 2 and 3D, we are interested in that due to Brezzi et al [3], because it uncovers crucial upwinding and conservation properties by simply interpreting the 1D scheme as a mixed method. To simplify the presentation, we deal with the stationary case ($D = 1$, $\chi = 1/\varepsilon$)

$$(3) \qquad \operatorname{div} \mathbf{p} = \operatorname{div} \left(\mathbf{grad}\, u + u\, \mathbf{grad}(\lambda/\varepsilon) \right) = f \quad \text{in } \Omega,$$

where the flux $\mathbf{p} := \mathbf{grad} u + u\mathbf{grad}(\lambda/\varepsilon)$ is a quantity of biological interest. Writing (3) in terms of the new unknown $u = \exp(-\lambda/\varepsilon)\, p$ leads to the following selfadjoint elliptic PDE with highly oscillatory diffusion coefficient

$$(4) \qquad \operatorname{div}(\exp(-\lambda/\varepsilon)\, \mathbf{grad}\, \rho) := f \quad \text{in } \Omega.$$

The idea is then to discretize (4) with a method that would account for rapid variations of $\exp(-\lambda/\varepsilon)$ and yield a positive definite symmetric M-matrix. For the method to be flux-preserving, that is to enforce continuity of the normal component $\mathbf{p} \cdot \mathbf{n}$ of $\mathbf{p}$ across interlement boundaries $e \in \mathcal{E}$, either mixed or hybrid finite elements are employed [2]. It is clear that (3) can be expressed equivalently as a system, namely

$$(5) \qquad \exp(\lambda/\varepsilon)\, \mathbf{p} - \mathbf{grad}\rho = 0, \qquad \operatorname{div} \mathbf{p} = f.$$

A mixed (or a hybrid) method approximates both quantities ρ and $\mathbf{p}$ at the same time. The method in [3] uses lowest order Raviart-Thomas mixed finite elements with Lagrange multipliers μ_T to relax the continuity constraint of $\mathbf{p} \cdot \mathbf{n}$. By static condensation the problem is reduced to an algebraic system with symmetric positive definite matrix (d_{ij}) for μ_T. The contribution d_{ij}^T of each element $T \in T$ to d_{ij} is

$$d_{ij}^T = \frac{|e_i|\, |e_j|}{\int_T \exp(\lambda/\varepsilon)}\, \mathbf{n}_i \cdot \mathbf{n}_j$$

2

where $\mathbf{n}_i$ is the external normal to the side e_i of T and $|e_i|$ is its length. We realize that if the partition T is acute, namely the internal angles of T are $\leq \pi/2$, then $\mathbf{n}_i \cdot \mathbf{n}_j \leq 0$ for $i \neq j$ and so (d_{ij}) is an M-matrix. The algebraic problem for μ_T corresponds to a linear nonconforming finite element approximation of (5) where the harmonic average $(\int_T \exp(\lambda/\varepsilon))^{-1}$ over T is taken instead of the usual average $\int_T \exp(-\lambda/\varepsilon)$. This property can be exploited for the purpose of implementation. Since $\mu_T|_e$ is a good approximation of ρ on $e \in \mathcal{E}$ [2], the following choice of u_T is justified as an approximate value for u on e [3]:

$$u_T|_e := \mu_T|_e \left(\frac{1}{|e|} \int_e \exp(\lambda/\varepsilon) \right)^{-1} \qquad \forall\, e \in \mathcal{E}.$$

The flux $\mathbf{p}_T$ can be computed afterwards, but this step is not mandatory if we are only interested in u.

We would like to conduct a preliminary study in 1D and get some insight on the mixed method, before embarking in a 2 and 3D implementation and related topological difficulties. In this particular but still relevant case, (d_{ij}) becomes tridiagonal and leads to the Scharfetter-Gummel scheme [3].

3. Streamline Diffusion Methods. This class of methods was introduced by Hughes and collaborators [6,7], and further studied and improved by Johnson and collaborators [5,8,9], for stationary problems:

$$(8) \qquad \mathbf{b} \cdot \mathbf{grad}\ u + a\ u - \mathrm{div}(\varepsilon\ \mathbf{grad}\ u) = F.$$

Time dependent problems can be handled easily with a *Discontinuous Galerkin Method*, which is based on a space-time finite element discretization with basis functions continuous in space and discontinuous in time. The time-step may vary not only in time but also in space [5,8,9]. We stress that in contrast to the previous method no advantage is taken now from the structure of the advection term $\mathrm{div}(u\ \mathbf{grad}(\lambda/\varepsilon))$ in (1), except for the obvious identification $\mathbf{b} = -\mathbf{grad}\ \lambda$ and $a = -\Delta\lambda$. This issue is to be explored further.

The basic idea consists of using a Petrov-Galerkin approximation with different spaces for trial and test functions, that introduces an upwinding in a variational context and copes with the main difficulty for advection-dominated problems: getting stability without sacrificing accuracy. Since there are several forms of the correction terms, we chose to discuss here that in [9]. For S_T being a space of continuous piecewise linear finite elements over a shape regular mesh T, the problem is to find $u_T \in S_T$ such that

$$(7) \qquad \int_\Omega (\mathbf{b} \cdot \mathbf{grad}\ u_T + au_T)(v + \delta\tilde{v}) + \dot{e}\ \mathbf{grad}\ u_T \cdot \mathbf{grad}\ v = \int_\Omega F(v + \delta\tilde{v}) \qquad \forall\, v \in S_T,$$

where

$$\tilde{v} := \mathbf{b} \cdot \mathbf{grad}\ v + av,$$

$$(8) \qquad \delta|_T := C_1 \max\left(h_T - \frac{\varepsilon}{|\mathbf{b}|}, 0 \right)/|\mathbf{b}| \qquad \forall\, T \in T,$$

$$\hat{e}|_T := \max\left(\varepsilon, C_2 h_T^2 |\mathbf{b} \cdot \mathbf{grad} u_T + au_T - F| \right) \qquad \forall\, T \in T.$$

This method is a clever variant of the usual Galerkin approximation and is obtained via two basic modifications. The streamline modification of the test functions from v to $v + \delta(\mathbf{b} \cdot \mathbf{grad} v + av)$ incorporates artificial viscosity only in the characteristic direction and can be interpreted as an upwinding mechanism that stabilizes the Galerkin scheme. That is however not enough to completely eliminate over and undershooting near discontinuities or transition layers. This is achieved via an artificial viscosity $\hat{e}$ depending on the "approximate" residual $R(u_T) := |\mathbf{b} \cdot \mathbf{grad}\ u_T + au_T - F|$ of the finite element solution u_T, because whenever $R(u_T)$ is expected to be large so is $\hat{e}$. This is the so-called shock-capturing correction. Unfortunately the resulting equations are nonlinear even for linear problems, which can be regarded as a price to be payed for stability and accuracy.

This method seems to be gaining popularity among practitioners in computational fluid dynamics mainly because it leads to similar results to finite difference schemes but offers more flexibility in terms of mesh adaptation and error control. In addition a number of important properties, such as local error estimates and crosswind smearing effect, are known for the simplified version without shock capturing but not for the finite difference competitors. We expect this project to contribute in clarifying virtues and drawbacks of this methodology, which can only be achieved with extensive analysis and numerical experimentation.

4. Mesh Generation. The ability to generate graded meshes that fit the structure of the underlying solution by placing more degrees of freedom (DOF) in regions of rapid variation is imperative for problems exhibiting *multiscales*. This, in conjunction with the above stable methods, would allow layer resolution for the physical quantities of interest, but without substantially increasing the global computational complexity.

We propose to use the automatic 2D mesh generator ADVFRONT of Paolini and Verdi [15], that has been successfully employed already for liquid-solid phase transitions in [12,13,14]. Given a mesh density function $h(x)$, ADVFRONT partitions Ω into shape regular triangles of size roughly $h(x)$ at location $x \in \Omega$, and the resulting mesh is guaranteed to be weakly acute. It can also produce elongated triangles, with large aspect ratios, oriented in a prescribed direction. This option is particularly appealing for problems exhibiting line singularities, for which triangles are to be aligned along them, thereby minimizing DOF in the tangential direction where the solution is varying slowly. Implementing flat triangles is a subject of intense research in the engineering community and has not yet received much attention in the mathematical one.

ADVFRONT is an *advancing front* algorithm that starts from the fixed boundary (or initial front) and successively adds triangles of size $h(x)$ to the current front until the entire domain Ω is triangulated. Choosing wisely the front segment, where a new triangle will be inserted, turns out to be essential in minimizing the front length. A few consistency tests have to be performed also to avoid front self-intersections as well as excessively close nodes. The computational complexity is dictated by those tasks. They are based on suitable *quadtree* data structures and binary search techniques that yield an overall quasi-optimal computational complexity of order $\mathcal{O}(J_T \log J_T)$, where J_T stands for the number of nodes of T [13]. The time our numerical experiments needed for mesh generation never exceeded 25% of the total CPU time [13].

5. A Posteriori Error Estimation and Adaptivity. If the discrete solution, say u_T, is a good approximation of the continuous solution, say u, then we may expect to detect interesting features such as transition layers by carefully postprocessing u_T. This extraction process is very popular in computational fluid and solid mechanics, and we refer to [1] for an account of methods and trends. For elliptic and parabolic problems there are a number of strategies to determine *a posteriori* error estimates. These are computable quantities at the element level, and thus inexpensive as compared with the solution process, that depend on the data and computed solution and provide lower an upper bounds for the error $u - u_T$ measured in suitable norms [1,9]. They are based on evaluating the strong form of the residual which consists of an element and a boundary or jump residual. Upper bounds show the *reliability* of the estimators, whereas lower bounds reveal their *efficiency*: no everestimation occurs. For advection-dominated problems the analysis is much behind due to intrinsic difficulties and the more recent development of reliable schemes, such as those in §§3 and 4 [5].

Solid-liquid phase transitions give rise to either sharp interfaces or narrow transition layers where the solutions change drastically. Even though their governing equations are different from (3), their numerical treatment pose similar questions about error estimation, layer resolution, and adaptivity. In [12,13,14] we have resorted to pointwise error estimators based on jump residuals (or discrete second derivatives) to equidistribute the interpolation error in space in the maximum norm and match it with the truncation error in time. This simple idea leads to *highly graded* and *noncompatible* meshes, together with savings in computing time for a desired accuracy.

Mesh admissibility tests are key ingredients for the success of an adaptive procedure. Once a mesh is rejected, then it has to be either adjusted to the new requirements of the flow or discarded, in which case

4

a new mesh must be generated. The latter is certainly an extreme but effective solution provided meshes are designed to last for a number of time steps, thus requiring more DOF. This is the alternative chosen in [12,13,14], which requires an efficient mesh generator such as ADVFRONT and reflects the trend in high performance computing that it is not wise to change mesh very often. Consequently estimation of interface or layer velocity becomes critical to predict their immediate location and design a mesh accordingly. Since consecutive meshes are not obtained via coarsening-enrichment strategies they are *noncompatible*, and so the problem of transfering information between them becomes nontrivial from the computational viewpoint. The proper balance between number of allowable mesh changes, refined region width, and element size cannot be achieved without careful analysis. These issues are addressed in [12,13,14] for the simplest liquid-solid phase transition, namely the two-phase Stefan problem, and research is now being conducted to extend this methodology to other phase transitions.

We intend to incorporate a posteriori error estimation in a later stage, that is when the model validation and parameter identification phases have been achieved. This would lead to a fully adaptive solver, capable of resolving features occurring at different scales with minimal computational effort and guaranteed error control. This topic was just a dream in solid mechanics a decade ago and is now becoming reality.

REFERENCES

[1] I. BABUŠKA, O.C. ZIENKIEWICZ. J. GAGO AND E.R. DE A. OLIVEIRA, *Accuracy estimates and adaptive refinements in finite element computations*, John Wiley and Sons, 1986.

[2] F. BREZZI AND M. FORTIN, *Mixed and Hybrid Finite Element Methods*, Springer, New York, 1991.

[3] F. BREZZI, I.D. MARINI, AND P. PIETRA, *Two-dimensional exponential fitting and applications to drift-diffusion models*, SIAM J. Numer.Anal., 26 (1989), pp. 1342–1355.

[4] I. EDELSTEIN-KESHET, *Mathematical Models in Biology*, The Random House/Birkhäuser, Mathematical Series, 1988.

[5] K. ERIKSSON AND C. JOHNSON, *Adaptive streamline diffusion finite element methods for convection-diffusion problems*, Math. Comp., 60 (1993), pp. 167–188.

[6] T.J.R. HUGHES. P. FRANCA. AND G.M. HULBERT, *A new finite element formulation for computational fluid dynamics: VIII. The Galerkin/least-squares method for advective-diffusive equations*, Comput. Methods Appl. Mech. Ingrg., 73 (1989), pp. 173–189.

[7] T.J.R. HUGHES AND M. MALLET, *A new finite element formulation for computational fluid dynamics: IV. A discontinuity-capturing operator for multimentional advective-diffusive systems*, Comput. Methods Appl. Mech. Engrg., 58 (1986), pp. 329–336.

[8] C. JOHNSON, *Numerical Solution of Partial Differential Equations by the Finite Element Method*, Cambridge Univ. Press, 1987.

[9] C. JOHNSON, *Adaptive finite element methods for diffusion and convection problems*, Comput. Methods Appl. Mech. Engrg., 82 (1990), pp. 301–322.

[10] A. MAJDA, *Compressible Fluid Flow and Systems of Conservation Laws in Several Space Variables*, Applied Math. Series 53, Springer, New York, 1984.

[11] D.M. MASON AND E.V. PATRICK, *A model for the space-time dependence of feeding for pelagic fish populations*, (to appear).

[12] R.H. NOCHETTO. M. PAOLINI. AND C. VERDI, *An adaptive finite element method for two-phase Stefan problems in two space dimensions. Part I: stability and error estimates*, Math. Comp., 57 (1991), pp. 73–108; Supplement, Math. Comp., 57 (1991), S1-S11.

[13] R.H. NOCHETTO. M. PAOLINI. AND C. VERDI, *An adaptive finite element method for two-phase Stefan problems in two space dimensions. Part II: implementation and numerical experiments*, SIAM J. Sci. Statist. Comput., 12 (1991), pp. 1207–1244.

[14] R.H. NOCHETTO, M. PAOLINI. AND C. VERDI, *A fully discrete adaptive nonlinear Chernoff formula*, SIAM J. Numer. Anal., 30 (1993), pp. 991–1014.

[15] M. PAOLINI AND C. VERDI, *An automatic mesh generator for planar domains*, Riv. Inform., 20 (1990), pp. 251–267.
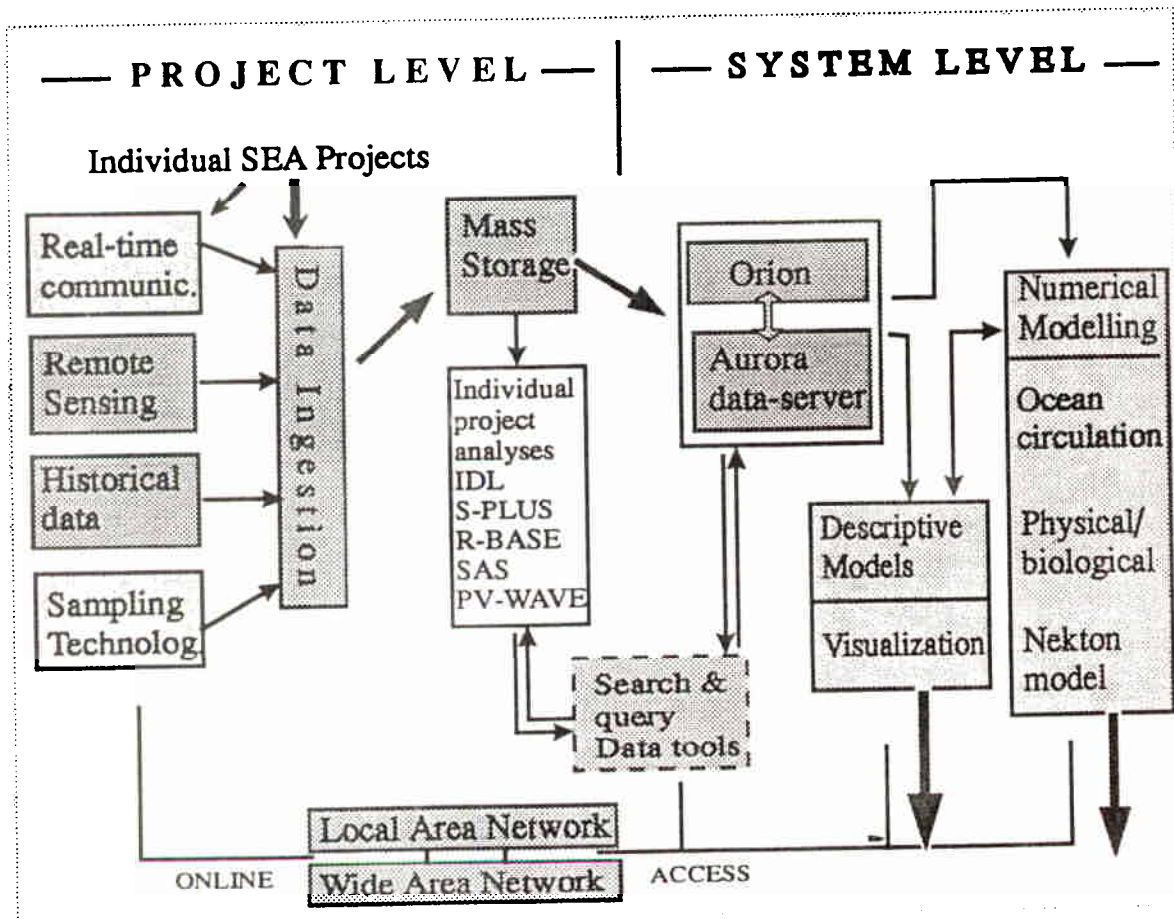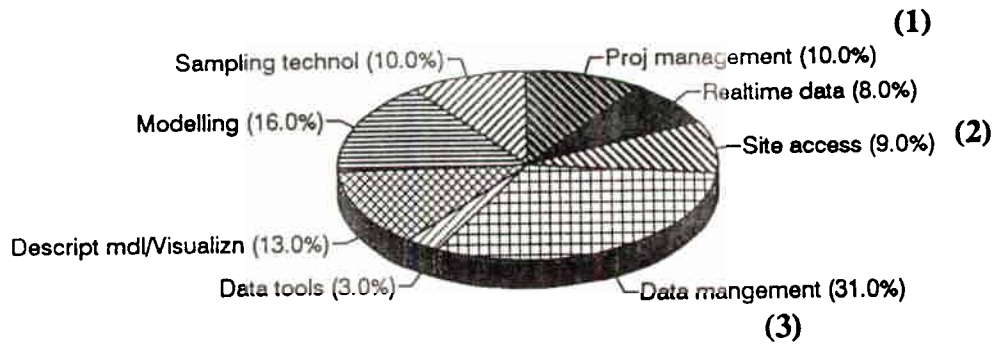
FIGURE 1: Structure of SEADATA
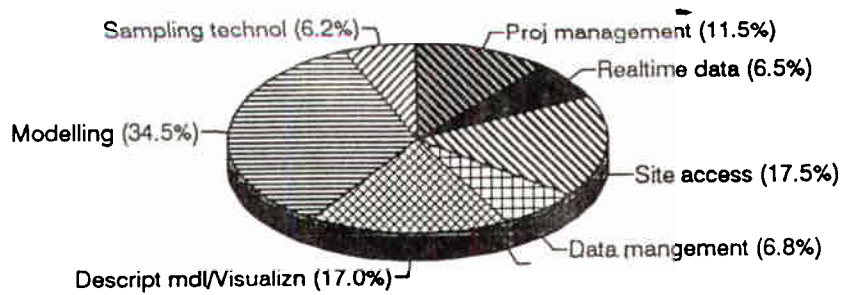
FY94

FY95

FIGURE 2: SEADATA budget breakdown by subproject for FY94 and FY95.

(1) Project management in FY95 includes annual audit charges.
(2) Data management includes hardware costs (workstations and storage devices); hence category is reduced in FY95.
(3) Site access includes circuit installation charges in FY94 and monthly Alascom and UACN circuit connection charges in both years (5.5 months @256kbs in FY94, 12 months @ 56kbs in FY95).

SEA Wide Area Network
components in place at end FY94

UAA

UACN   Fairbanks

Anchorage

leased
terrestrial
line (256kbs)

UAF

router

csu-
dsu

satellite
T1

NWNET   Seattle

NSFNET

Alascom

satellite
256kbs

INTERNET

csu-
dsu

Dial-in access
by modem from
regional
communities

CTC

possible future extension

router

?

bridge

PWS
Community
College

Director/Admin
SEAOCEAN
SEAFISH
SEADATA
WetLab
Visitors
Education
GIS
OSRI

PWS Science Center

Cordova

Data
Server

router

csu-
dsu

p.gain

LAD

LAD

CTC

CTC

p.gain

router

p.gain

bridge

ADF&G

Library

T1

Near realtime
data
communications
system

CTC

Cordova
community
access

csu-
dsu

PWSSC
Orca

FIGURE 3: SEA Network Connections
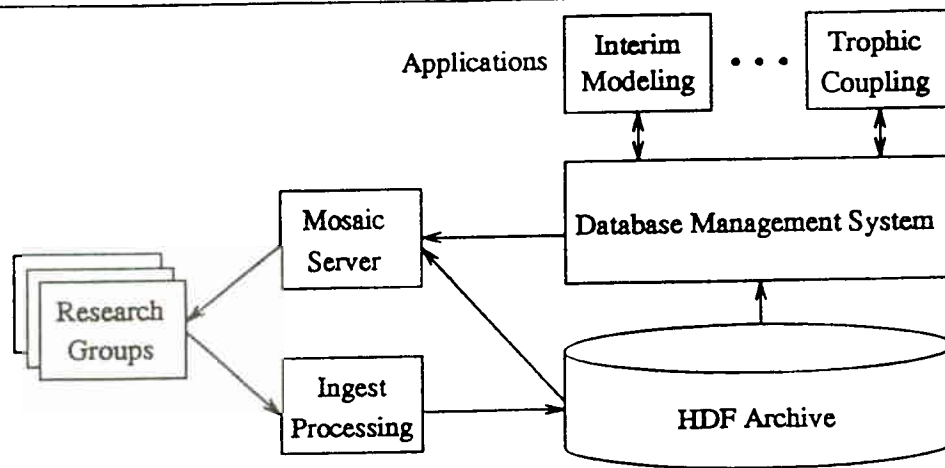
FIGURE 4a: Proposed data management architecture using HDF archive and relational DBMS
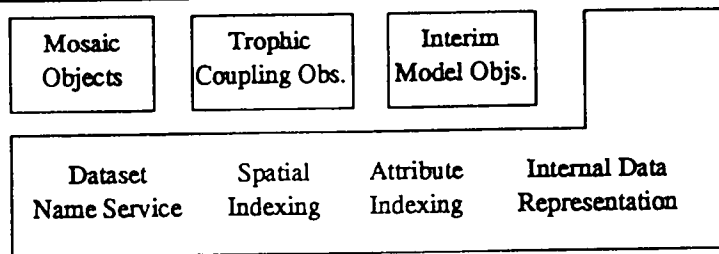
FIGURE 4b: The database components for general and application-specific functionality
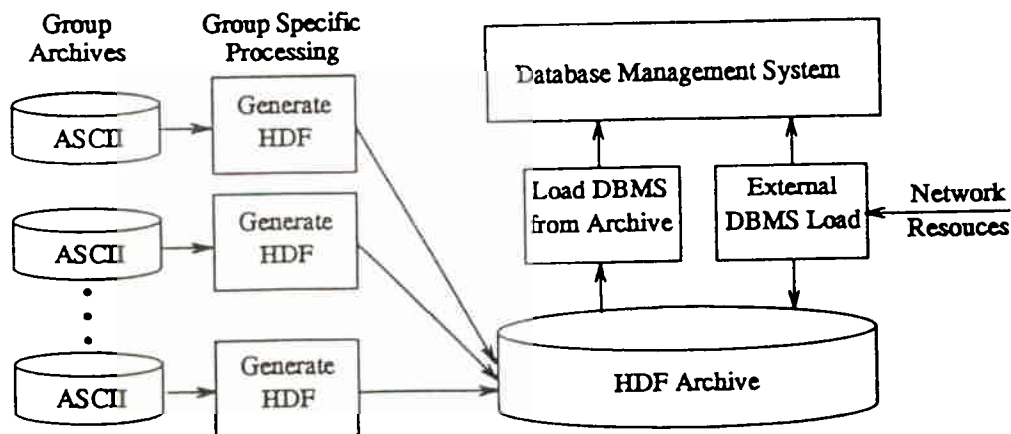
FIGURE 4c: The ingest processing component of the data management architecture.
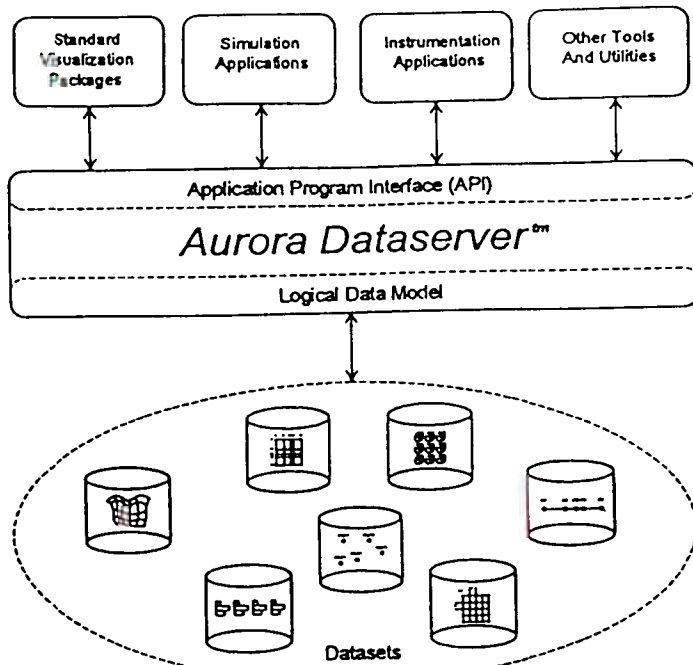
FIGURE 5: Structure of the Aurora dataserver.
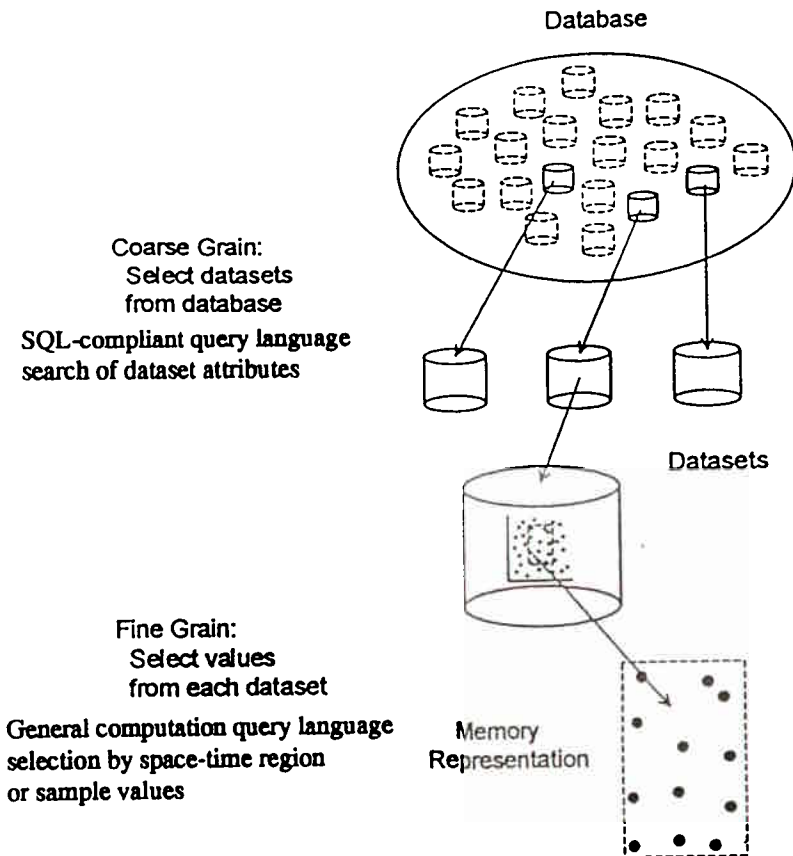
FIGURE 6: Coarse-grain / fine-grain retrieval system in Aurora
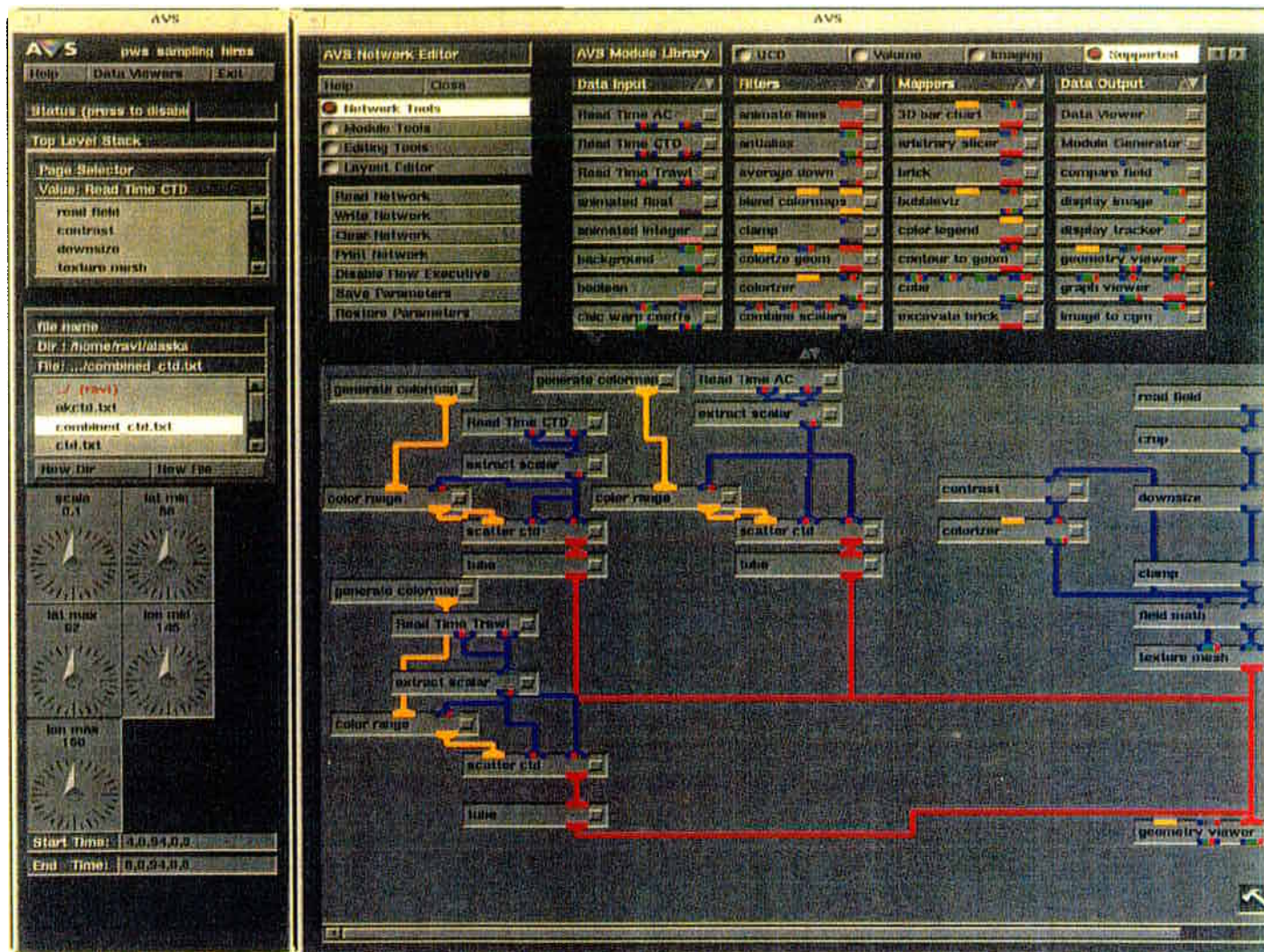
FIGURE 7: AVS "network" interface for viewing SEA sampling locations for multiple projects within specified time and spatial bounds. This network generated the image shown in Figure 8.

FIGURE 8: AVS image of the "western corridor" showing all sites sampled between June 15 and July 15, 1994, by CTD (vertical columns), hydroacoustics (horizontal lines), and midwater trawl (open circles).
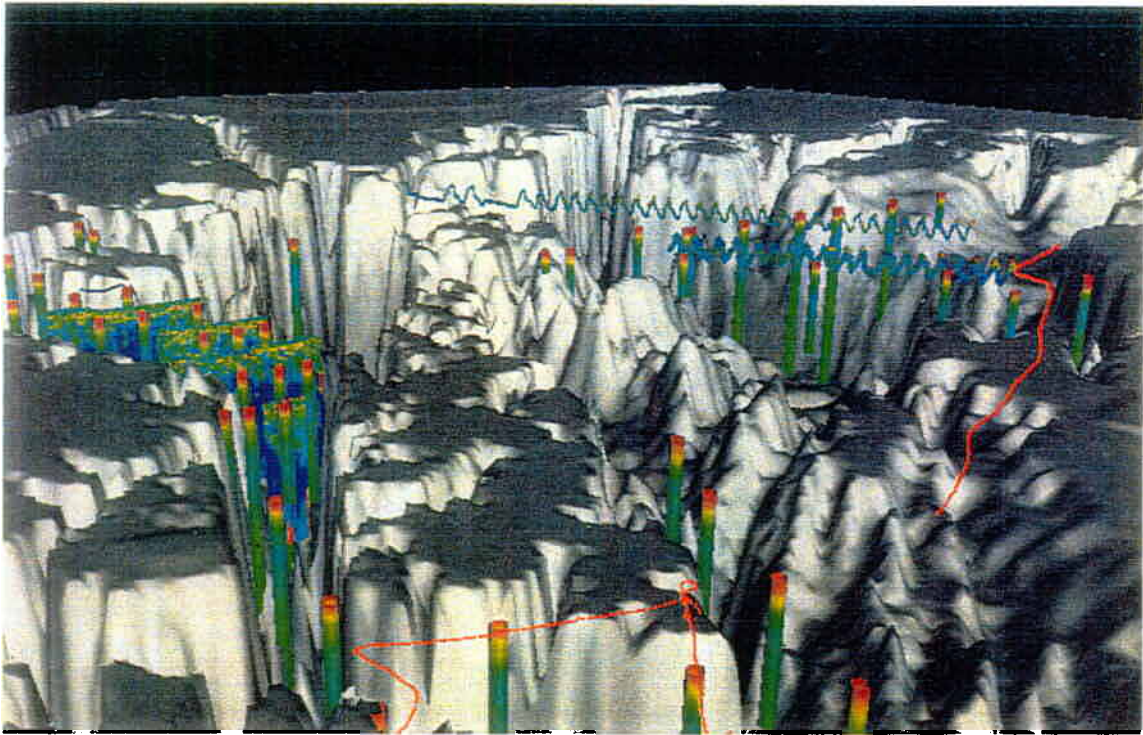
FIGURE 9: AVS image of western PWS, Knight Island in foreground, showing selected CTD-temperature data (vertical columns), hydroacoustic transects (vertical sheets), aquashuttle trajectories (undulating lines), and aerial flight paths (red lines).
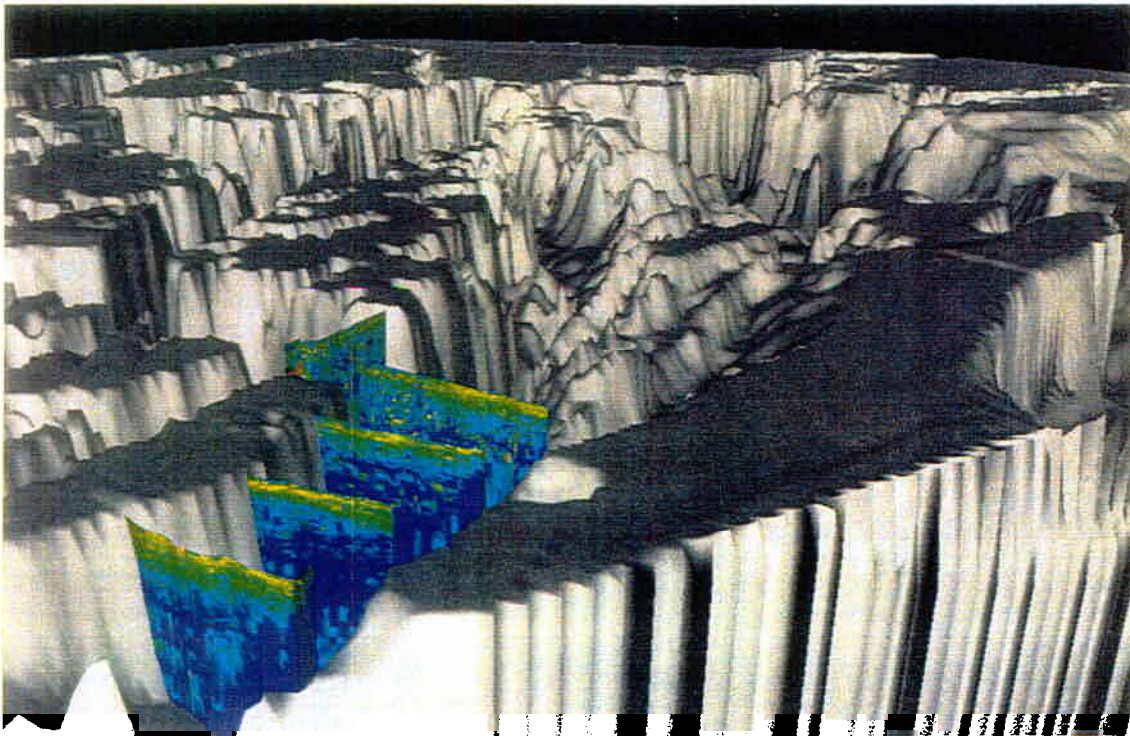
FIGURE 10: Closeup of hydroacoustic transects in Montague Strait.
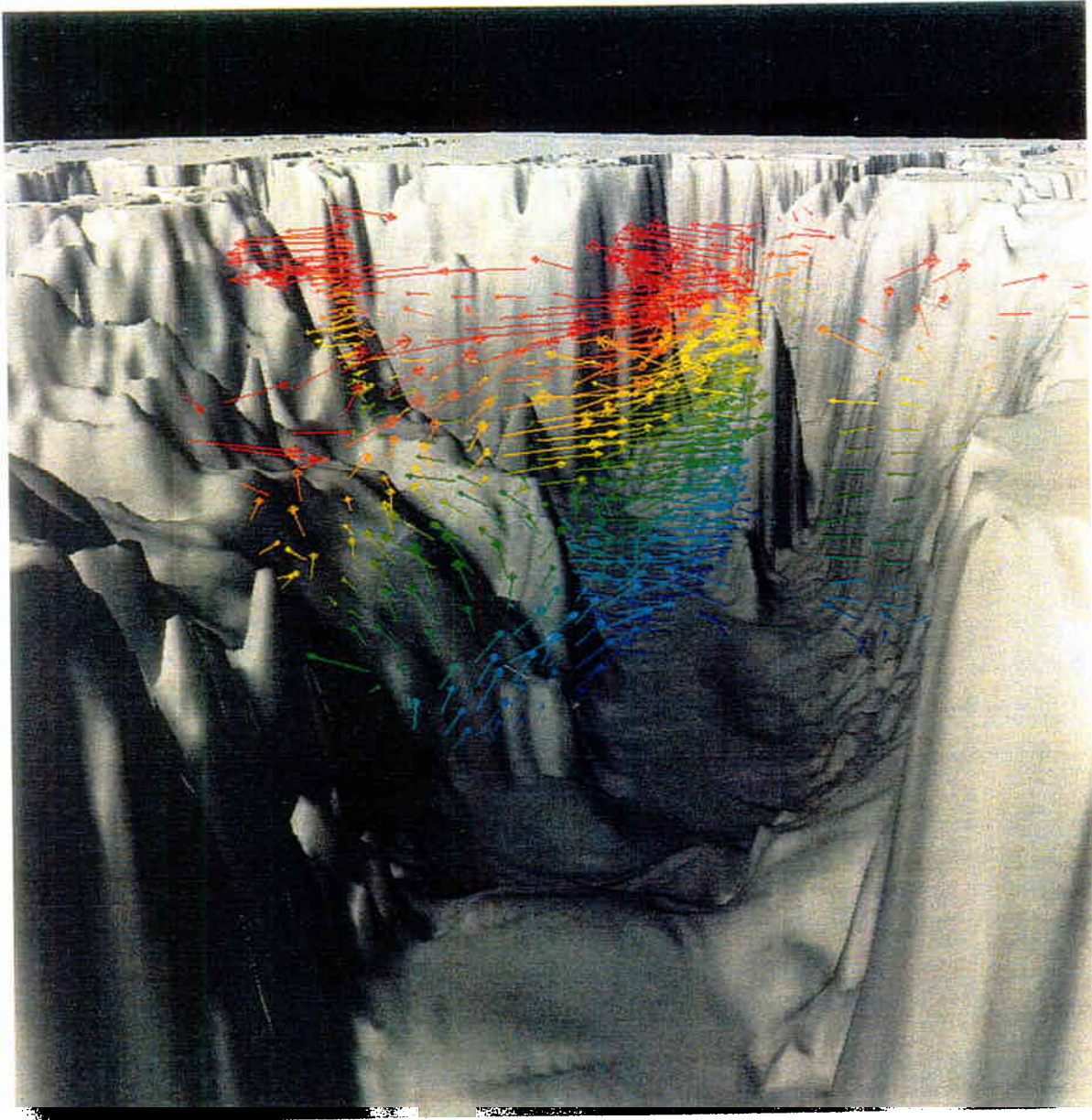
FIGURE 11: ADCP current vector data from central PWS

variability in the physical structure of the water column over time. We are also examining spatial variability in zooplankton distributions in relation to physical oceanography within PWS and the adjacent coastal GOA. In the long term, the zooplankton and physical oceanography databases developed in this study will be used in conjunction with historical information to address the Lake-River, Prey-Predator, and Herring Overwintering hypotheses put forth in the original SEA plan (SEA, 1993).

We have designed a self-contained subsurface mooring to be deployed in the Hinchinbrook Entrance region. The mooring will contain a CTD, ADCP and acoustic modem/release for data transmission. We anticipate that the time series derived from these instruments will help to address problems pertaining to deep water renewal and replenishment of oceanic zooplankton stocks in PWS. The data set derived from the mooring promises to be the highest resolution (year round information) set available for characterizing temporal (and within the context of the water column, spatial) variability in the flow through Hinchinbrook Entrance. We are experimenting with the possibility of utilizing ADCP backscatter (sea truthing the backscatter with nets) to characterize variability in the hypothesized advection of zooplankton stocks into PWS.

We have obtained and/or updated numerous historical data sets for PWS and the North Pacific. These include upwelling indices, North Pacific sea level pressure, North Pacific sea surface and air temperatures, and the Southern Oscillation Index for various periods between 1881 and 1994.The analysis of these data sets will be aimed at addressing the river-Lake hypothesis, as well as characterizing how PWS and the GOA vary interannually in relation to large scale oceanic and atmospheric forcing (i.e. phenomena such as the El Nino Southern Oscillation cycle, nodal tidal cycle, and interannual variations in the 3-4 and 5-7 year range that might be connected to tropical variability or be part of oscillations intrinsic to the greater North Pacific region. We have nearly completed a manuscript examining long term changes in the extratropical North Pacific wind, and sea surface temperature fields.

We have entered into an informal cooperative relationship with the U. S. Coast Guard, in which they have consented to allow scientists onboard USCGC Sweetbrier. In addition the Coast Guard has devoted vessel time strictly for the purposes of conducting oceanographic research operations. Data collection included CTD, ADCP, optical plankton counter and nutrient chemistry. Thus far we have participated in two cruises. We would like to see further and expanded cooperative efforts of this kind during FY 95. We have also received a donation of 16 Seacat CTDs from British Petroleum, to further support our oceanographic data collection efforts. We also recently had a proposal accepted by the Alyeska Ship Escort Response Vessel System to tow our ADCP in Port Valdez and the PWS tanker traffic lane to greatly refine our knowledge of the temporal variability of the ocean currents in these regions of PWS. Finally, we participated in a cooperative effort with NOAA Sea Grant and the Institute of Marine Science at the University of Alaska to install a thermosalinograph on the tanker Keystone Tonsina. The vessel transits PWS and the GOA four times a year on a Valdez to Honolulu transect of the North Pacific. The data obtained from this component of the study will be useful in characterizing seasonal and interannual variability in PWS and the GOA, and how it is related to changes in the

greater North Pacific, through the subarctic transition zone into the subtropical gyre.

We feel that the 1994 SEA physical oceanographic program has been very successful in every aspect, and we plan on using what we learned this year to improve and focus our 1995 data collection, with the goal of advancing our understanding of how the physical environment constrains the ecology of Prince William Sound. The 1995 SEA physical oceanographic program promises to be a very productive and intensive field effort, coupled with integration and synthesis with other data sets from within and outside of the SEA program. We plan on publishing numerous physical oceanographic and interdisciplinary articles in the peer reviewed literature. The results and figures presented in this report are not to be cited or published elsewhere without written permission from the authors.

Introduction

A description and understanding of the physical environment is integral to the definition of an ecosystem and therefore, the oceanography of PWS must be included in any study which proposes to identify and understand ecosystem level processes in PWS. From the two primary hypotheses which form the foundation of the SEA plan (the river-lake hypothesis and the prey-switching hypothesis), it is possible to derive two primary objectives of the oceanography component in the SEA plan. They are: 1) identifying physical forcing of the production dynamics in PWS with particular emphasis on the exchange of nutrients and plankton between PWS and the GOA (river-lake hypothesis), and 2) uncovering oceanographic factors which mediate prey switching between calanoid copepods and juvenile pink salmon fry (prey-switching hypothesis). To achieve either one of these two above objectives we must develop and expand our knowledge on the basic oceanography of the Sound in terms of its hydrography, mixing, and circulation properties. These objectives, form the primary focus of the physical oceanographic component of the SEA plan.

Data and Methods

During 1994, we collected and processed conductivity/temperature/depth (CTD) data from approximately 950 locations in PWS and the GOA. Much of the data was collected during five cruises between April and September of 1994. The data also include a collection of 4 year long time series begun under the Cooperative Fisheries Oceanographic Study (CFOS) program. The CTD information used in this study was collected during April, May, June, July and September of 1994. Spatial coverage was greatest during June, July and September. During April and May the work was concentrated in western PWS. Figure 1 shows a collection of CTD stations that is representative of our 1994 sampling scheme. Neither the ADCP data nor the computed velocity estimates from the CTD data are presently corrected for the effects of tides.

For collecting direct ocean current information, we used a 150 kHz broad band acoustic doppler current profiler (ADCP), deployed off the side or stern of the vessel in a towed body. Once we removed a dysfunctional paravane system, the towing configuration proved to be quite stable in terms of pitch and roll, neither of which exceeded 5 degrees during most of the towing operations. When bottom depths exceeded 400 m, we were able to continue to track bottom by lowering the instrument further into the water column. The ADCP was towed at speeds of up to 6 knots and the instrument was able to track bottom down to over 400 m when the vessel moved at slower speeds. A reference layer depth of 200 m was used in the deepest regions of PWS (~ 800 m) when depths exceeded bottom tracking range. We used 4 meter bin depths for our vertical sampling resolution for most of the cruise. The data presented here were averaged in time for periods between 120 and 660 seconds. The instrument was delivered to us by the manufacturer in early September, so that ADCP data was collected only on our September cruise.

We have developed and standardized algorithms and structures for data storage, processing and analysis in the UNIX environment. In many cases, these methods are much more powerful than those written specifically for the hardware for use in a PC environment.

Results and Discussion

The following abstract represents a summary of the large scale circulation patterns and physical property distributions in PWS and the GOA. Following the abstract we briefly report on some of the highlights of our data analysis for the winter. The full manuscript (Salmon et al., 1995) that contains these and numerous other results is available to EVOS peer reviewers on request. Finally, we include the abstract and a few figures from a data report summarizing the results of regional physical oceanographic measurements in a number of embayments in western PWS.

Abstract:

Hydrography and Circulation in Prince William Sound, Alaska during Spring, Summer, and Fall of 1994

CTD data taken during spring, summer and fall of 1994 show that in the deepest regions of the Sound the vertical distributions of salinity and temperature can each be divided into three distinct regions, a seasonal thermocline and halocline in the upper 100 m, a main thermocline and halocline between about 100 and 450 m, and a very weakly stratified, constant temperature deep layer between 450 and 750 m. The upper 150 m of the Sound is consistently cooler and less saline than the upper 150 m of the adjacent Gulf of Alaska. Deep water renewal is apparent in the spatial distributions of temperature and salinity below 150 m during June and July. These saline waters have been advected throughout northern and northwestern PWS by September. A temperature minimum exists at the bottom of the seasonal thermocline in the central and northwestern regions of PWS. The minimum warms by 0.5°C between April and late July, after which it begins to cool, and the depth varies with the season from 45 m to 115 m. This minimum is not present at the entrances to the sound, nor does it occur in the adjacent coastal waters. A small subsurface temperature maximum occurs at 300 m in the central and northwestern sound during April and May. By June the maximum has eroded and was not observed in July or September.

Analysis of ADCP data collected during September 1994 considerably refines what is known of the circulation in the central basin of PWS. The large scale flow in the central basin can be described as a two layered system in which the upper layer (upper 150 m) and subsurface (150 - 400 m) velocities oppose each other. Upper layer velocities are up to 30 cm/s, while subsurface velocities are on the order of 5 to 10 cm/s. ADCP measurements in the central region of PWS show that the cyclonic circulation cell that exists here during fall is essentially restricted to the upper 150 m. The surface cyclone also exists in the winter months, as evidenced by AVHRR imagery. The ADCP data often show that circulation in the Sound is characterized by numerous counterflows, both in the horizontal and the vertical. Some ADCP profiles show surface and subsurface current structures that appear to be closely associated with topography. Horizontal flow, both near surface and deep is sheared in the central sound and the entrances to it. The amplitude and spatial structure of computed baroclinic geostrophic currents are in general agreement with currents directly observed with the ADCP.

The measurements reported in this paper were undertaken as part of the Sound Ecosystem Assessment (SEA) program that began in PWS during 1994. SEA is an interdisciplinary study aimed at understanding variability in Pacific herring and pink salmon populations in PWS within the context of variability in plankton populations, predator populations and climatic forcing. The initial physical oceanographic surveys have been aimed at describing spatial and temporal physical property variations in PWS, and how they interact with, and are forced by, variability in the GOA. We are particularly interested in characterizing and understanding variability of deep water processes because of their potential relationship to variability in oceanic macrozooplankton populations (calanoid copepods) that inhabit PWS and live below 300 m during most of the year. These populations are very important to the ecology of many pelagic fish species in PWS, particularly during the short period of their life history (usually April and May) in which these zooplankton inhabit near surface waters in PWS. Similarly, we seek to discern the spatial and temporal patterns of variability in physical structure and properties of the near surface waters because strong relationships exist on interannual time scales between the abundance of oceanic macrozooplankton populations and variations in the strength of the upper layer flow regime in PWS during spring.

We briefly present a few results and figures that exemplify the different types of analyses we undertook during 1994.

Figure 2 shows the distributions of temperature and salinity (T/S) at standard depths (20 m to 750 m) in PWS and the adjacent waters of the GOA for the period April 21 through July 22 1994. The curves through the data were constructed by averaging all of the observations in a particular region at each depth, and then fitting a smoothed curve to the averaged values. Waters in the Knight Island Passage, North West Sound, and Central Sound regions share similar T/S characteristics, including a prominent temperature minimum occurring near the 31.7 psu isohaline surface. No subsurface temperature minimum is apparent at the Hinchinbrook Entrance, South West Sound or GOA CTD stations. The Hinchinbrook Entrance and Montague Strait (South West Sound) stations have T/S properties that are intermediate between those of the adjacent GOA and the waters of the interior region of PWS. The GOA stations are consistently warmer than those in the interior sound as well as those at Hinchinbrook Entrance and Montague Strait.

Figure 3 is a time series of mean temperature versus salinity curves at standard depths in northwest PWS. Again, the mean curves represent smoothed fits to the spatial mean of all the CTD stations in the region. The time series shows seasonal changes both near the surface and at depth. Near surface (at 20 m) salinities decrease as summer heating brings more freshwater discharge into PWS both locally and through advection in the ACC. Variability in temperature and salinity is substantially higher in the surface layer from 0 m to 10 m (not shown). Similarly, mean near surface temperatures increase from about 4.5°C to 7.0°C with increasing insolation. A subsurface temperature minimum occurs near the 25.1 σ_t isopycnal surface (salinity ~ 31.7 psu), and increases from 4.2 to 4.7°C between April and July as it moves deeper into the water column. The depth of the minimum varies between about 40 m and 115 m between April and

July. This minimum occurs over most of the northwestern Sound and all across the central PWS basin (figure 4).

The distribution of temperature across PWS and in the ACC at 20 m during July shows the effects of the ACC in the upper layer circulation (figure 5). The warmer ACC waters can be seen moving in through Hinchinbrook Entrance and sweeping north and west on the eastern limb of the cyclonic surface gyre. The ACC does not penetrate into western PWS, but appears to exit PWS through Montague Strait. Temperatures in the upper 50 to 150 m within PWS are consistently cooler than those in the upper layer of the Hinchinbrook Entrance region just outside of PWS and upstream in the ACC. Similar spatial patterns occur during June, July and September in the upper 150 m.

An east to west temperature gradient exists in the deep water during June, July and September in which the waters in Hinchinbrook Entrance and central PWS are warmer than Knight Island Passage and western PWS (figures 6 and 7). The gradient monotonically decreases in time between June and September. During June, the maximum temperature difference between the eastern and western sections of the Sound at 250 m is about 0.4°C, while in September it has decreased to less than 0.1°C. Much of the variability in Hinchinbrook Entrance and the central basin of the Sound is attributable to the direct interactions between Hinchinbrook Entrance and the warmer waters of the GOA. Similarly, the spatial homogeneity of the Knight Island Passage and western PWS waters is partly due to their isolation (due to topography) from these direct interactions with the GOA.

At 350 m during July, there is a very small east-west gradient in which the waters below the surface cyclone in the central region of the sound are more saline than those in western PWS (figure 8). This pattern may be a seasonal one, in the sense that the deep saline inflow that has been advected into the central Sound during summer has not yet penetrated into the western sound by late July. By the end of September, salinities at 350 m have increased by 0.2 to 0.3 psu in Knight Island Passage and western PWS, indicating that the deep water has been replaced, ostensibly because summer deep inflow from the GOA has been advected throughout the main interior basin of the Sound. As a result, there is a north to south gradient in the distribution of salinity at 350 m during September.

Vertical salinity distributions for the deepest regions of the sound (> 400 m) show three distinct regions of salinity gradient (figure 9). The seasonal halocline is characterized by large changes in the upper 20 m. The amplitude of the salinity gradient fluctuates in phase with the regional fresh water cycle. A weak main or permanent halocline occurs from about 20 m to 400 m. The gradient in this region is about 4×10^{-3} psu/m as salinities change by approximately 1.5 to 2.0 psu over 350 to 400 m of the water column. Below the main halocline there is a layer of very weakly stratified water with salinities of 33.0 - 33.07 psu between 460 and 750 m. The gradient (2×10^{-4} psu/m) in this layer is more than an order of magnitude smaller than that in the region lying directly above it.

There are also three regions that characterize the vertical temperature profiles (figure 10) in the deepest sections of PWS. The seasonal thermocline extends to 50 m in April, warms and deepens to a maximum depth during late May and early June and continues to warm into July. The main thermocline extends from 50 - 100 m (fluctuates from April-July) to about 300 m. The vertical gradient in this region is +0.006°C/m. The temperature increases by 1.25°C - 1.5°C over 200 to 250 m of the water column in this region of the thermocline. This section of the water column represents a transition zone from the colder glacially influenced northern PWS derived surface waters and the warm deep waters advected in from the GOA. At about 350 to 400 m, a small (~ 0.02°C) local temperature maximum occurs during April and May. Between 400 m and 750 m the temperature is nearly constant at 5.67°C. It is not clear whether this isothermal and nearly isohaline water mass is fully or partially replaced during summer deep water renewal each year. Nutrient and oxygen measurements to be made during 1995 will refine our understanding of deep circulation in the Sound.

ADCP data show that circulation in the Sound is characterized by numerous counterflows, both in the horizontal and the vertical. ADCP transects across the central basin of the Sound show that the deep flow in this region is closely tied to the topography (figure 11). The main portion of the deep inflow to PWS moves north and west, while there are regions of opposing flow directly adjacent to the topography on all sides of the basin. The counterflows near the lateral boundaries occur on both the latitudinal and longitudinal transects of the basin. The central basin transect from Zaikof Point to Bligh Reef shows a westward moving current that is in contact with the topography of Montague Island. This inflow could be the incoming tide from the GOA moving in through Hinchinbrook Entrance and continuing northwestward around Montague Island.

Figure 11 shows the flow switching direction several times over the course of the transect, both in the upper layer and deep flow. The near surface cyclonic flows to the northeast for approximately 15 km along the transect, after which the flow becomes west-northwest for about 20 km along the transect. Maximum velocities of approximately 30 cm/s occur in the near surface flow at a depth of 25 m. The velocity field at 200 m along this transect is generally opposed to that in the near surface region. The amplitude of the flow at 200 m is on the order of 5 -15 cm/s for both the westward and eastward components. Over most of the transect, the near surface flow pattern extends to about 150 m. The amplitude of the velocities decreases continuously with depth in most cases, though there are a few sections that show subsurface velocity maxima. The surface to 150 m northeast flow is underlain by west velocities from 150 m to 300 m, while the region with surface west-northwest flow is characterized by eastward velocities from 150 m to the bottom at 400 m.

We computed baroclinic geostrophic velocities for several regions, including those that were directly sampled with the ADCP. The geostrophic approximation is not completely valid within the confined waters of PWS, especially in the constricted passages and entrances. Even so, the computed velocity distributions are qualitatively similar to the direct measurements in regions such as Hinchinbrook Entrance (figure 12). In the central basin of the Sound, where the geostrophic approximation is more likely to hold (or nearly hold), the computed geostrophic

velocities agree well with direct measurements, both in amplitude and in the spatial pattern of the flow fields. These data suggest that the upper layer cyclonic circulation is coherent down to about 200 m. Maximum upper layer velocities are approximately 65 cm/s for both the computed geostrophic and direct ADCP velocity estimates in the central Sound between Naked Island and Hinchinbrook Entrance.

The ADCP data show complicated current structures in Hinchinbrook Entrance and Montague Strait that are at least in part due to the tides. We are unable at this point to fully resolve the tidal and nontidal components of the flow in these regions, but our preliminary examination of the flow fields is nonetheless enlightening. In Montague Strait the entire water column moves northward on the flood, with maximum currents of over 40 cm/s in the upper 45 m. Approximately halfway through the transect the tide turned and began to ebb. The apparent response of the currents to the tide change is manifested by 10 to 25 cm/s southward flow in the upper 40 m. In Hinchinbrook Entrance, the surface flow seems to be more strongly controlled by tides than is the deep flow. The upper layer currents change directions with the tide, while the current remains northward from about 60 m to the bottom during both flood and ebb tide suggesting that the mean flow is northward into PWS through Hinchinbrook Entrance over the course of the tidal cycle.

Bering Explorer Cruise, consecutive stations, Sept. 1994
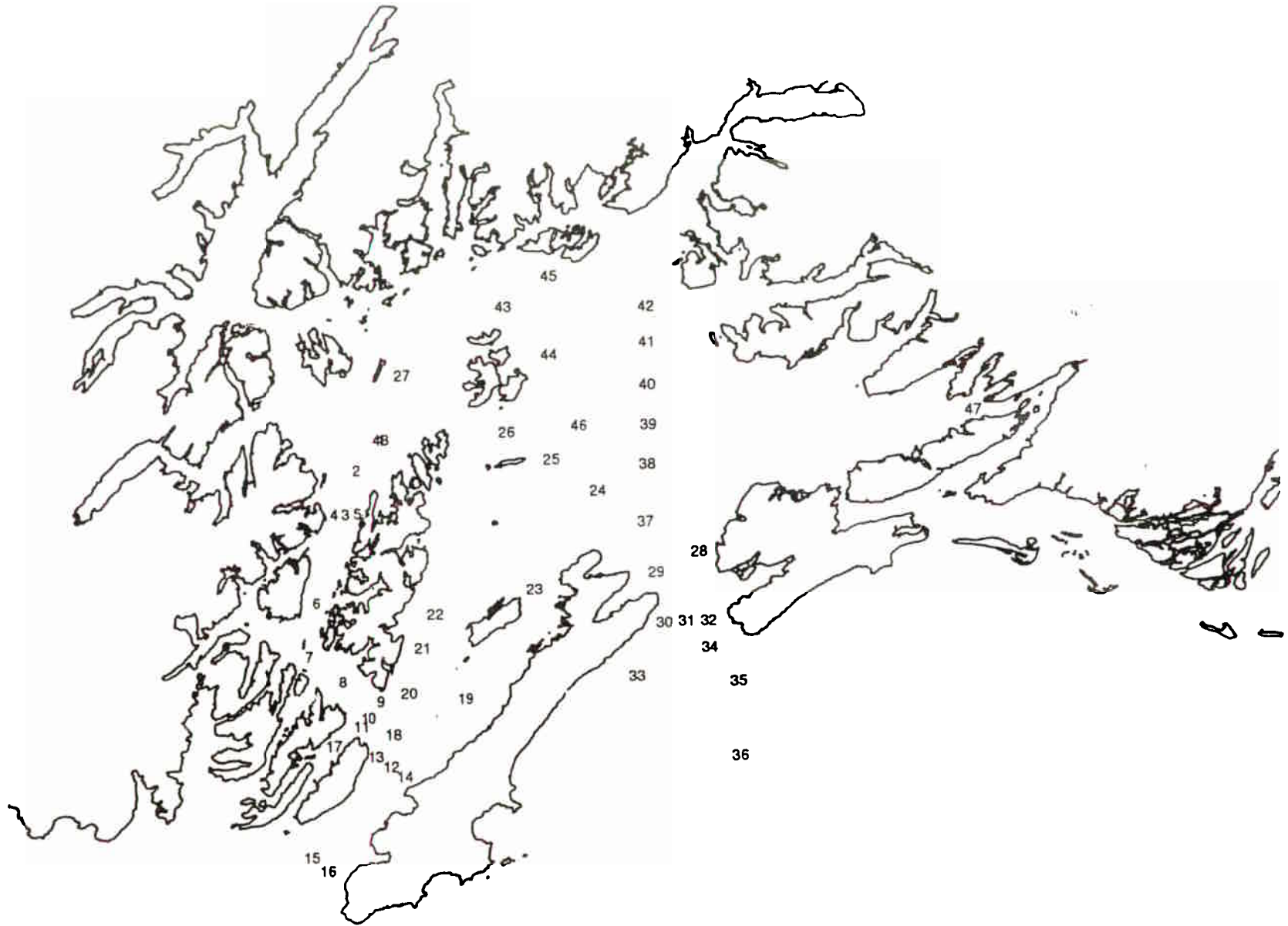
Figure 1) Map of representative CTD stations in Prince William Sound and the adjacent Gulf of Alaska.
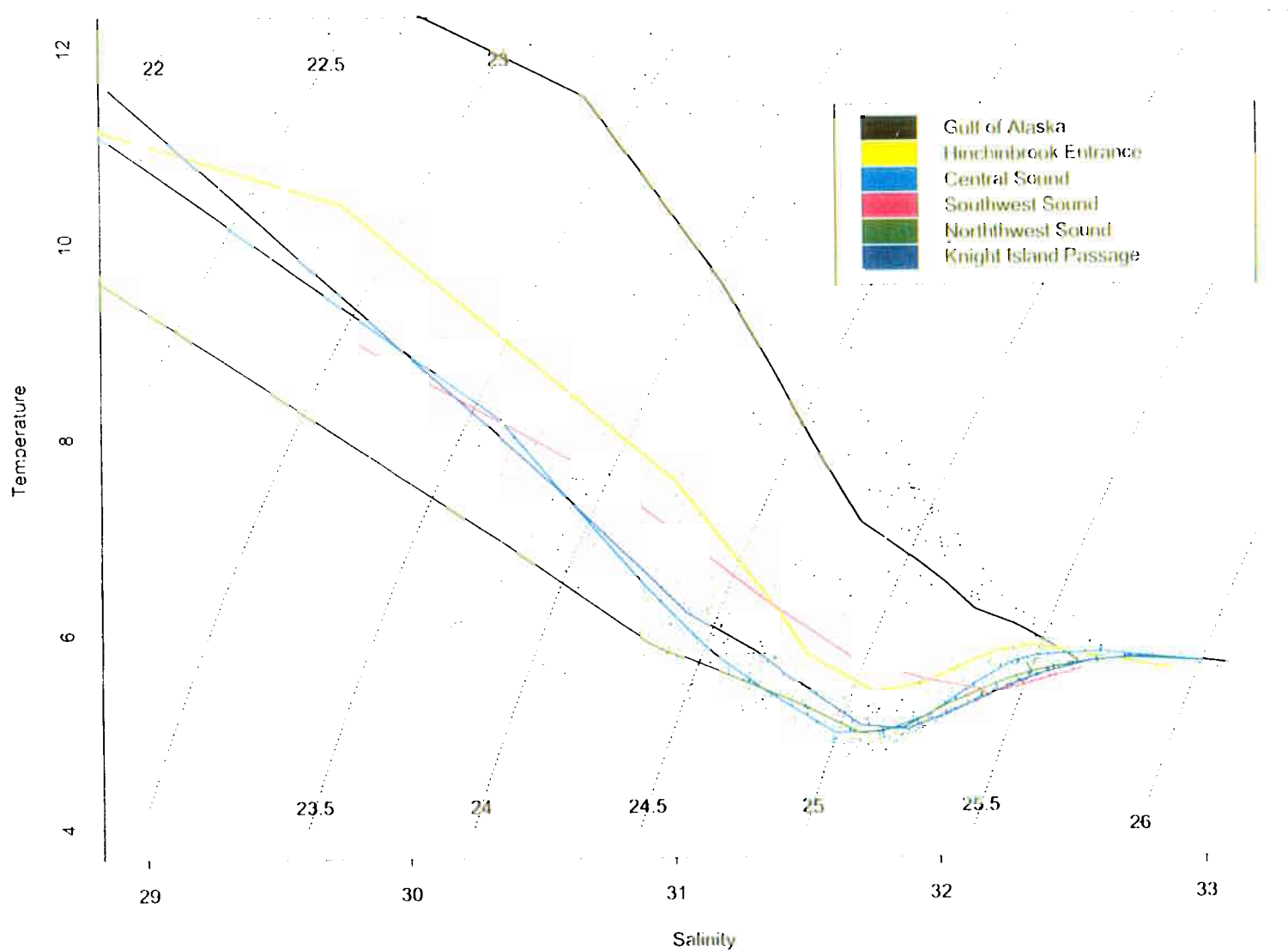
Figure 2) T/S curves for various regions of Prince William Sound and coastal Gulf of Alaska for the month of July. Three distinct water types are evident. Salmon et al. data not to be published or cited elsewhere without written permission.
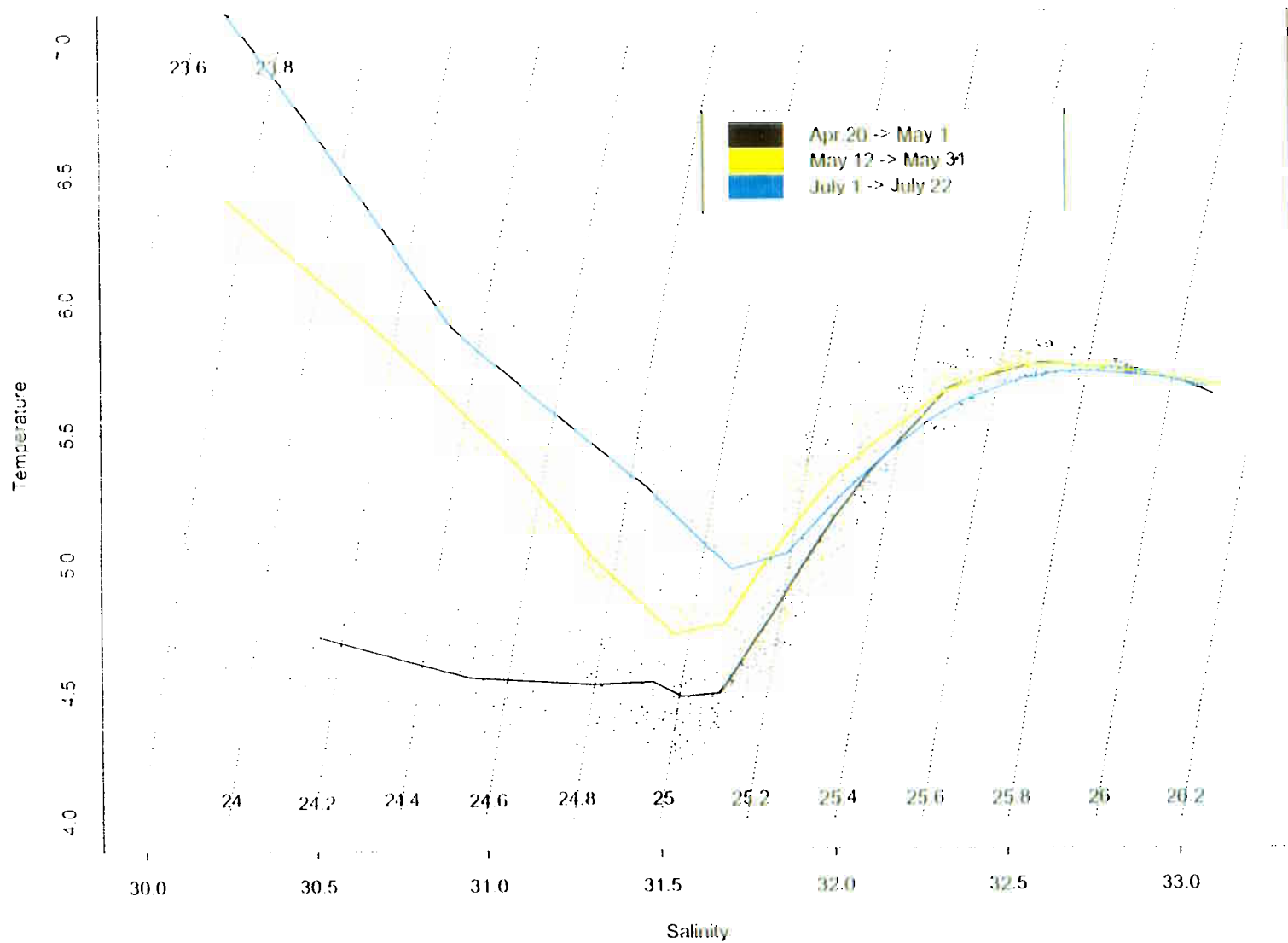
Figure 3) Time series plot of T/S in northwestern Prince William Sound showing onset of seasonal heating, freshening and changes in the depth of the vertical temperature minimum.

Central Sound Transect, 07/20/94, Temperature
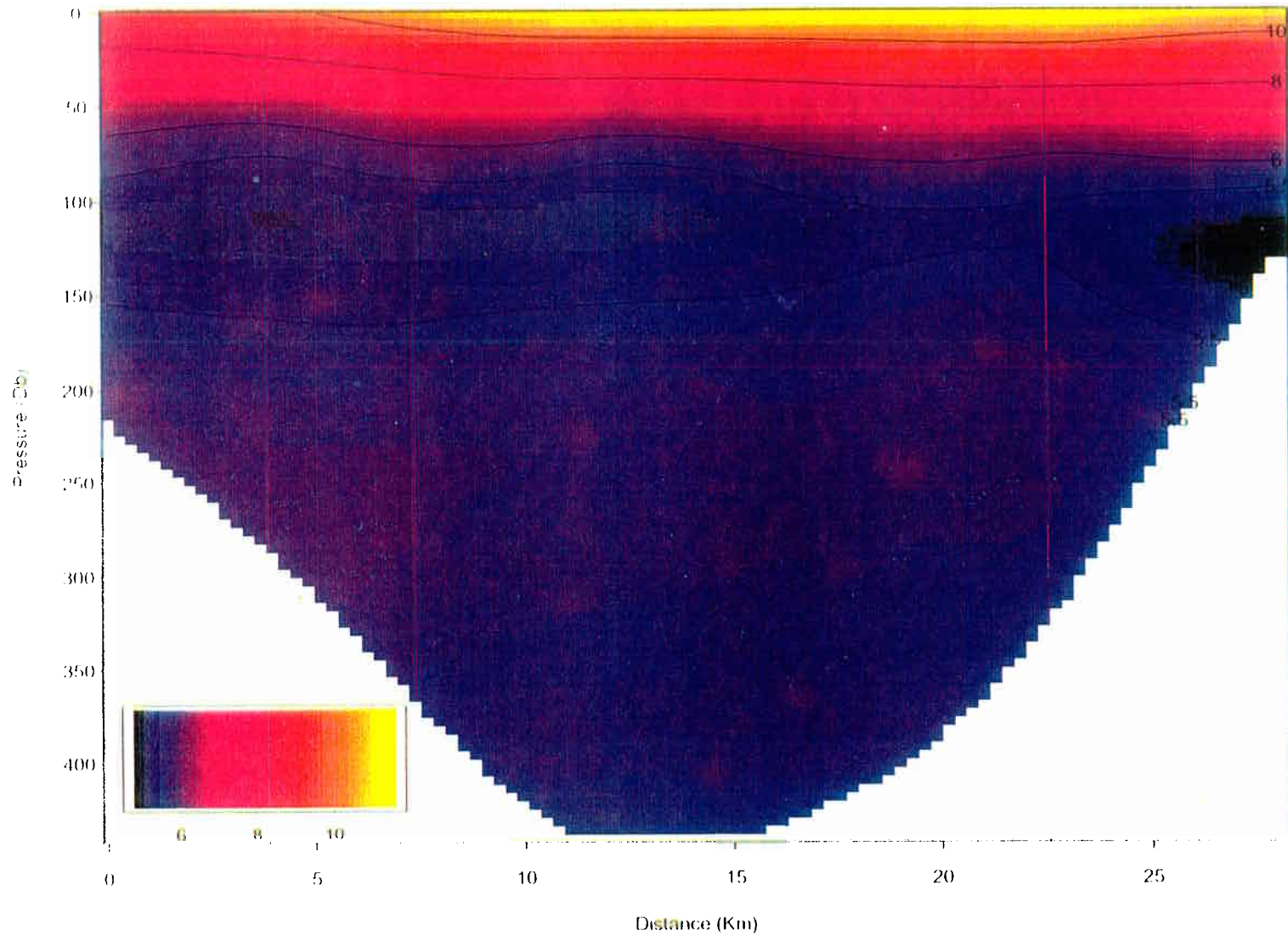
Figure 4) Transect through the central basin of Prince William Sound illustrating the ACC in the upper layer and the large spatial scale of the vertical temperature minimum. Salmon et al. data not to be published or cited elsewhere without written permission.
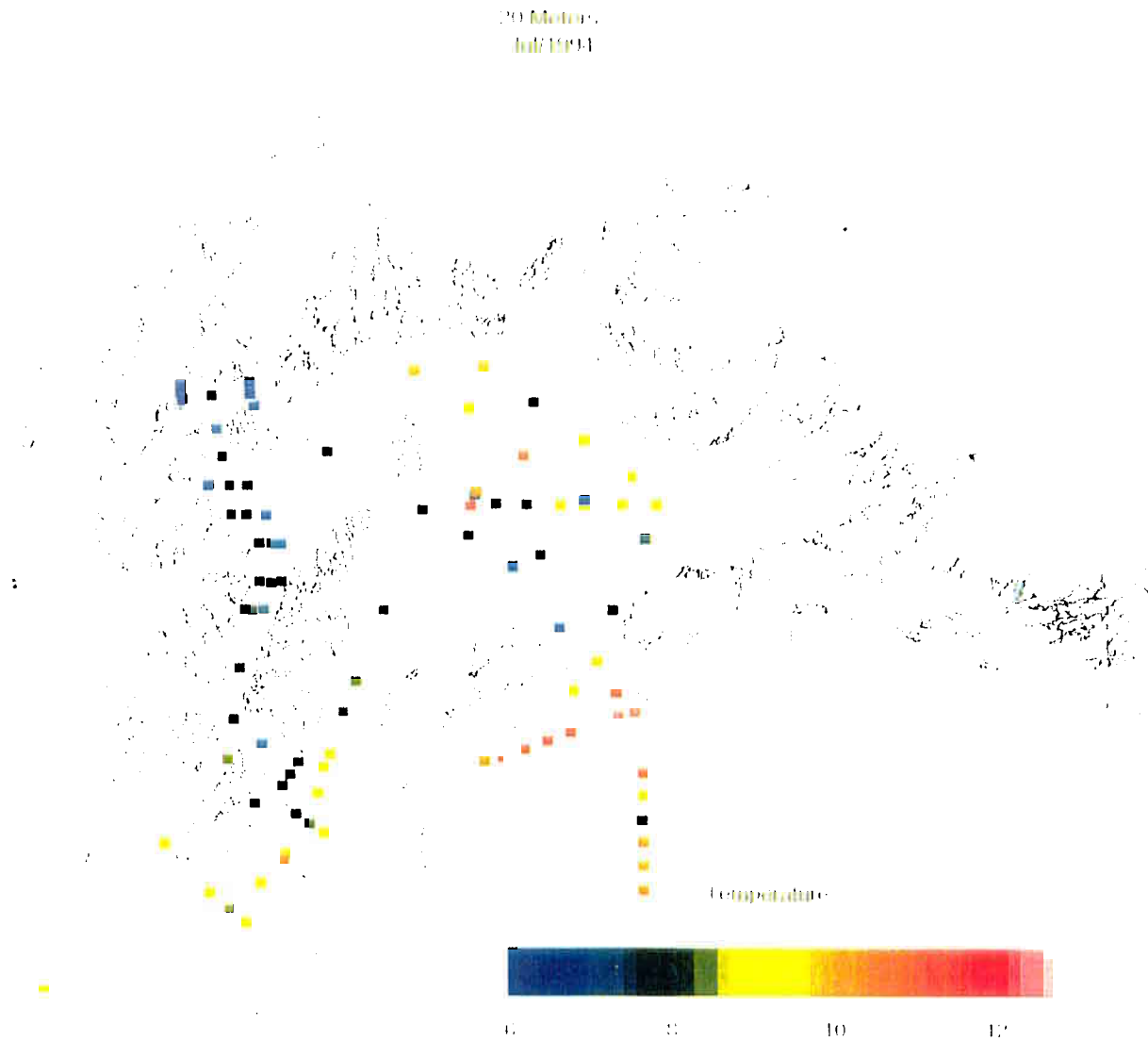
Figure 5) Temperature scatterplot at 20 m during July showing the ACC flowing in through Hinchinbrook Entrance, transiting the central basin of the Sound and exiting through Montague Strait. Salmon et al. data not to be published or cited elsewhere without written permission.
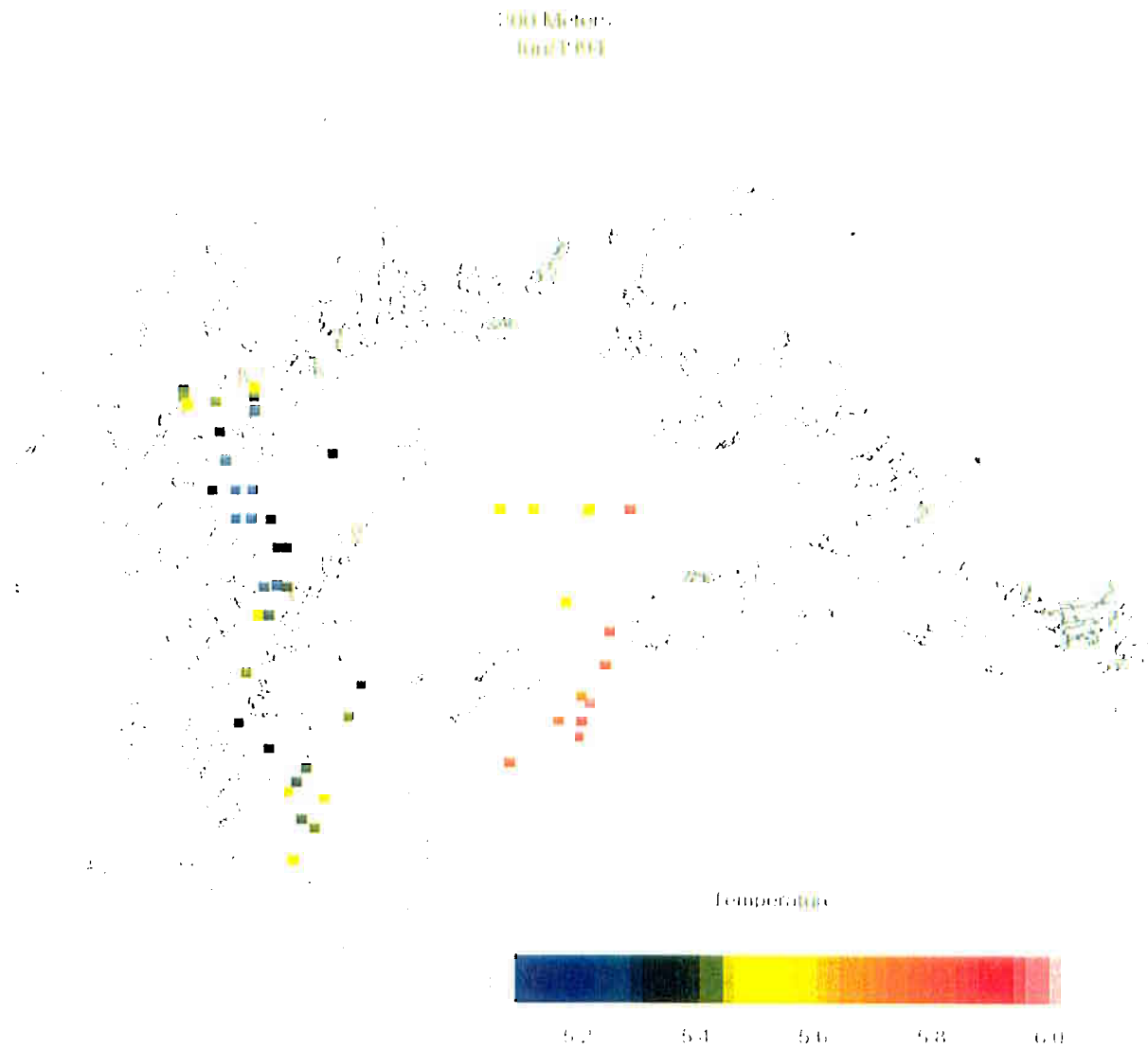
Temperature

Figure 6) Temperature scatterplot for the deep layer at 200 m during June illustrating various aspects of summer deep water renewal. Salmon et al. data not to be published or cited elsewhere without written permission.
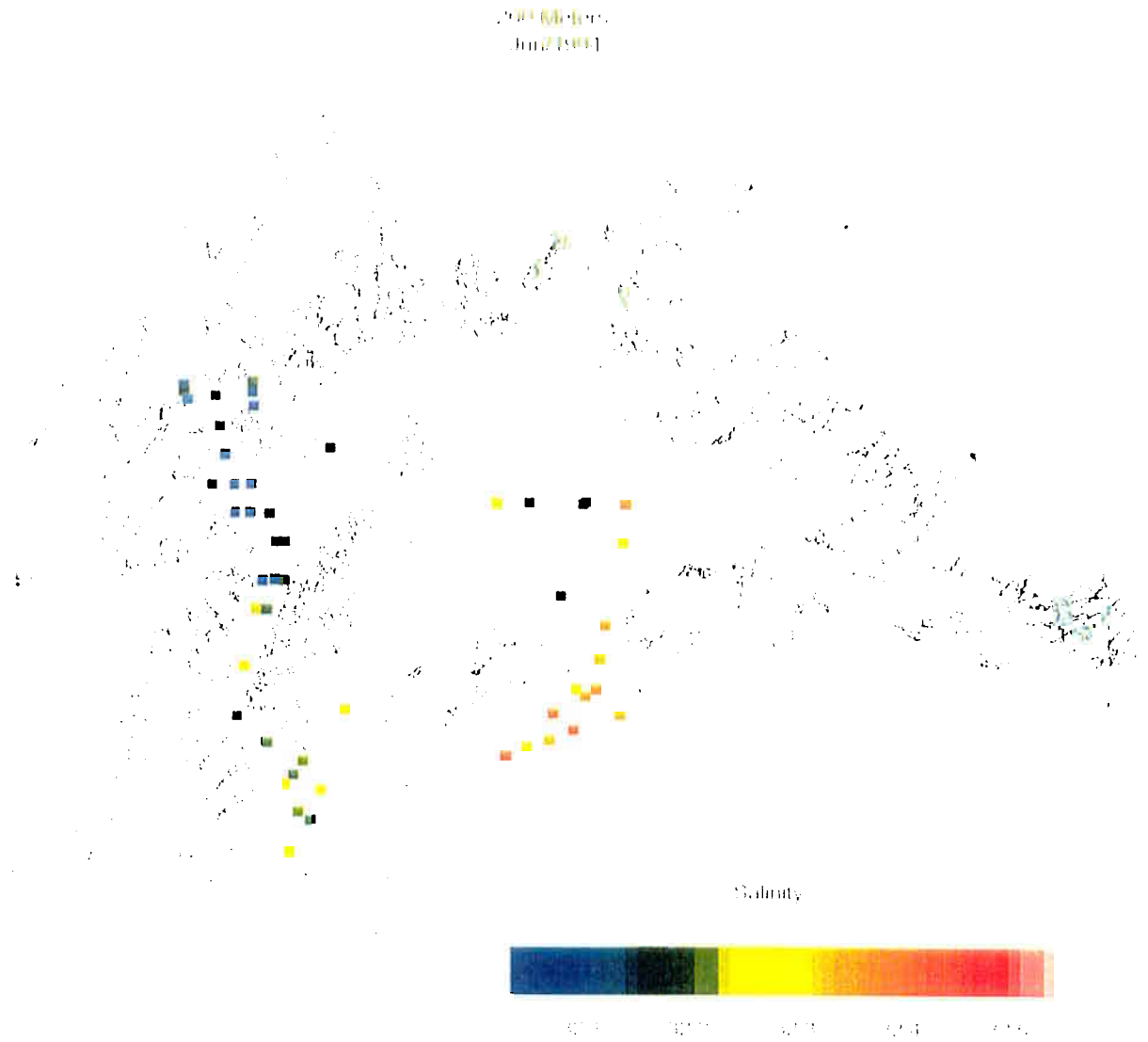
Figure 7) Salinity scatterplot at 200 m during June showing extent of intrusion of warmer Gulf of Alaska derived waters at depth. Salmon et al. data not to be published or cited elsewhere without written permission.
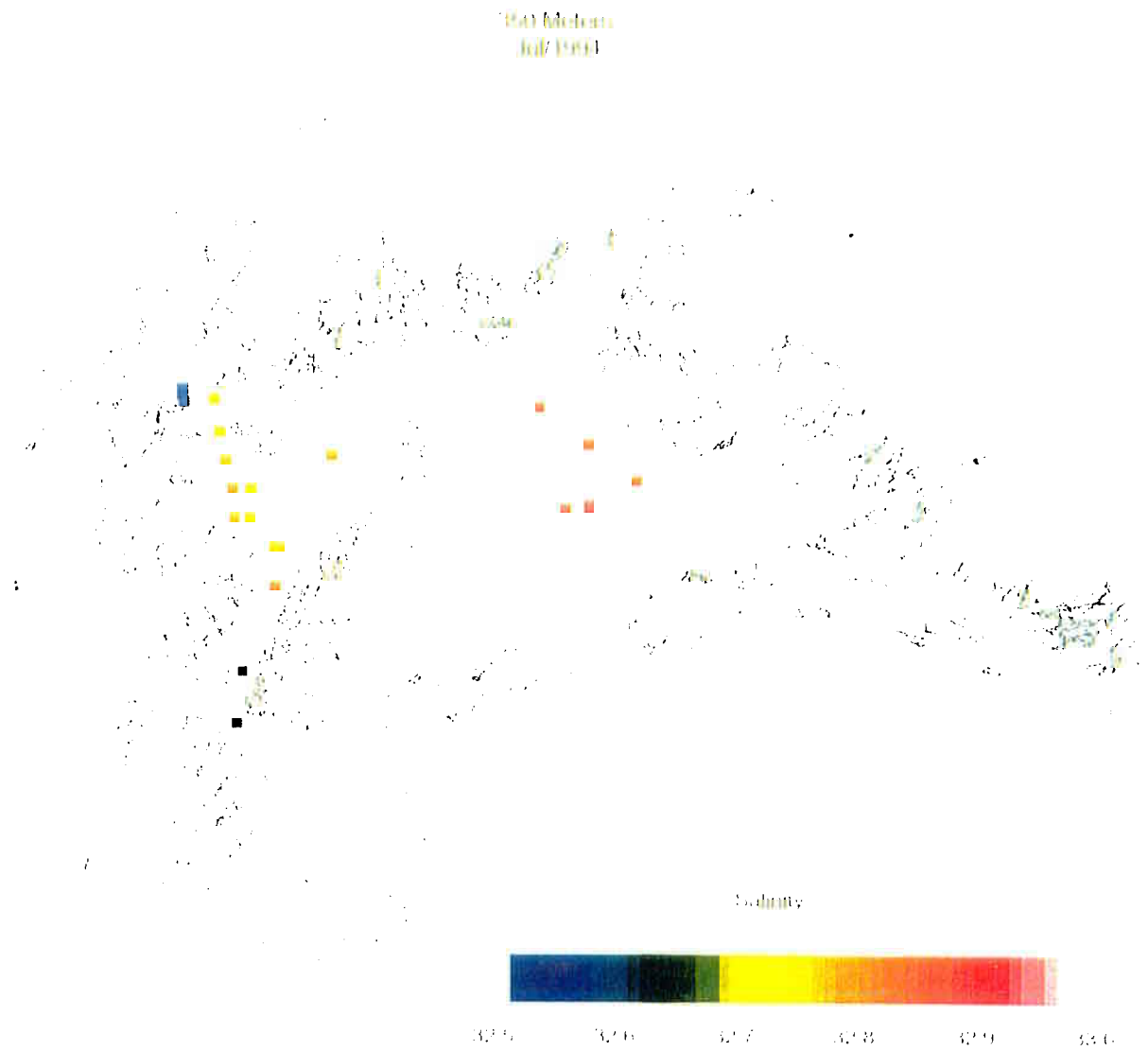
Figure 8) Salinity scatterplot at 350 m during July showing deep water renewal occurring in the central Sound. Salmon et al. data not to be published or cited elsewhere without written permission.
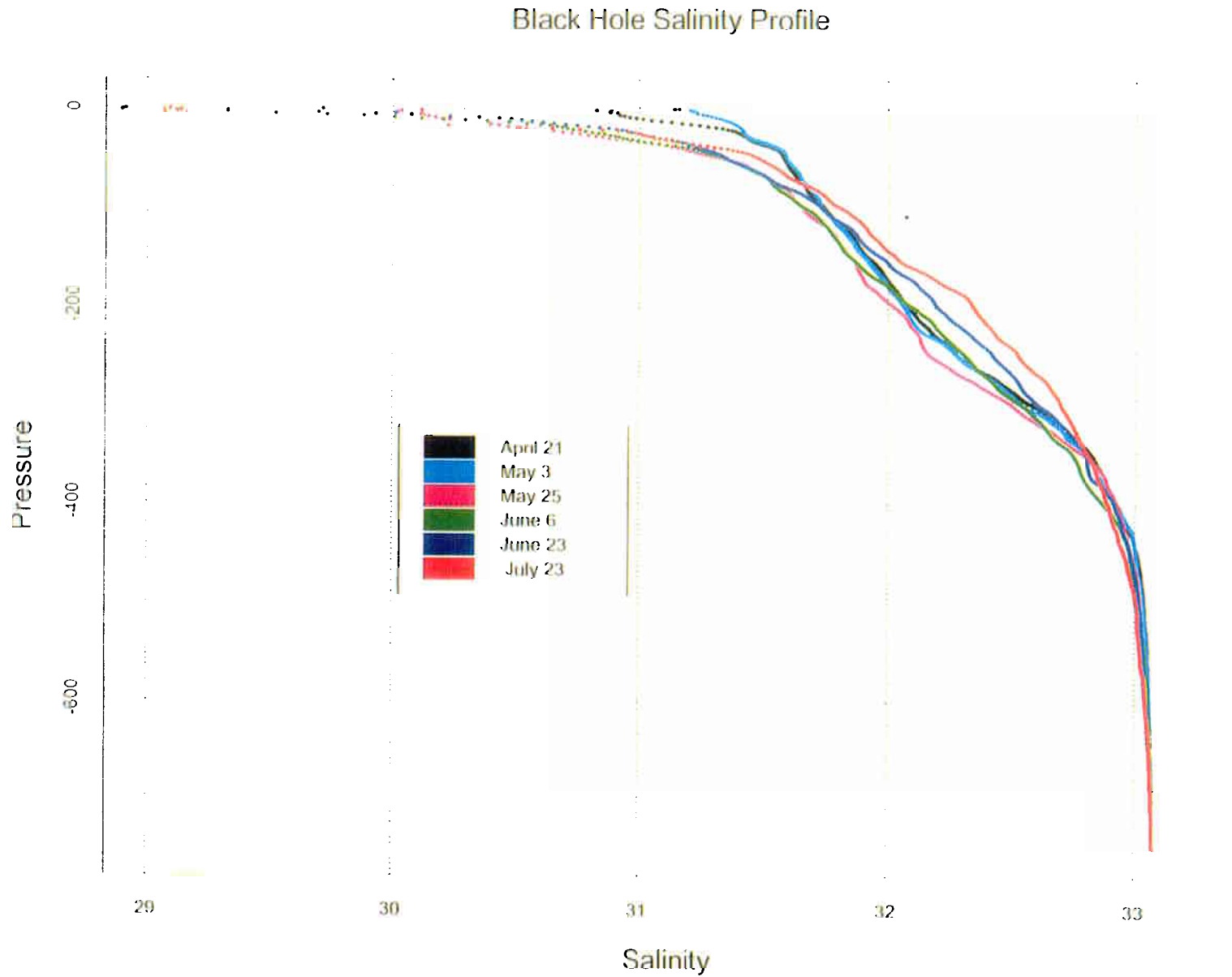
Figure 9) Salinity profiles from the northwestern Sound ("Black Hole") April to July, showing three distinct regions in the vertical structure. Salmon et al. data not to be published or cited elsewhere without written permission
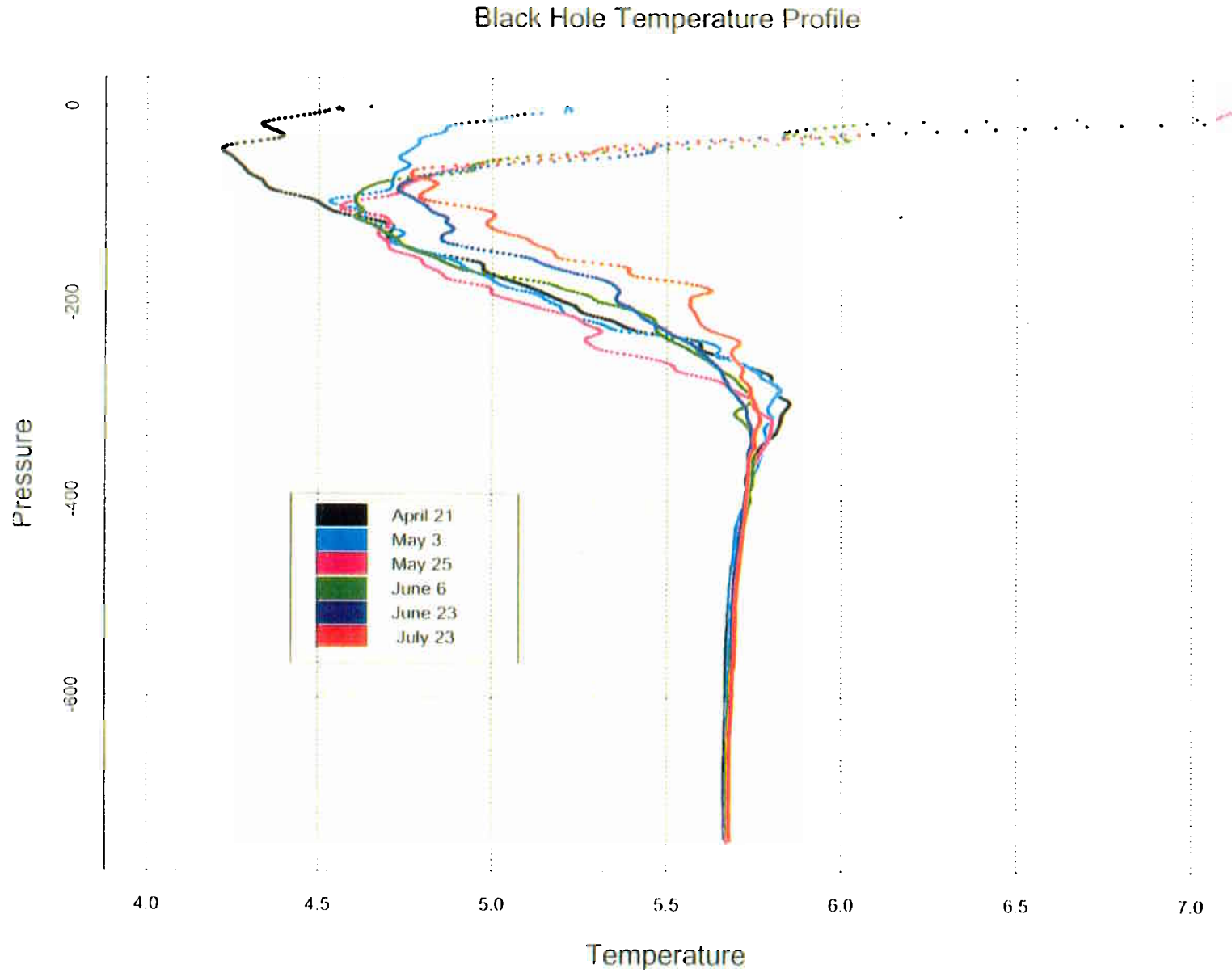
Figure 10) Temperature profile from the northwestern Sound ("Black Hole") time series April to July showing three distinct regions in the vertical structure. Deep water is nearly isothermal. Salmon et al. data not to be published or cited elsewhere without written permission
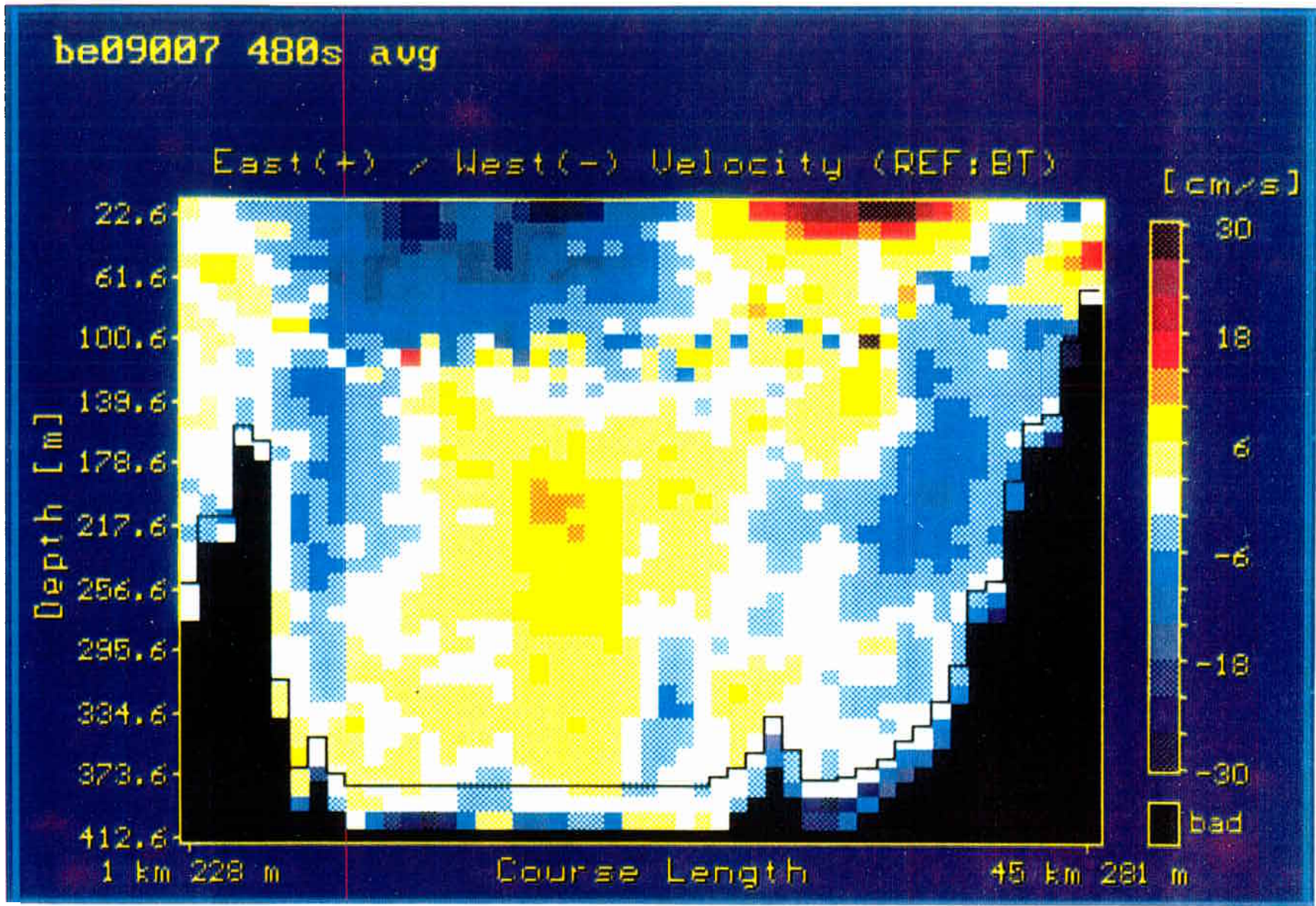
Figure 11) East-west velocities from ADCP illustrating counterflowing vertical currents. Salmon et al. data not to be published or cited elsewhere without written permission.

Figure 12a) Relative velocities of baroclinic geostrophic flow in Hinchinbrook Entrance. Southward velocities are negative. Salmon et al. data not to be published or cited elsewhere without written permission.
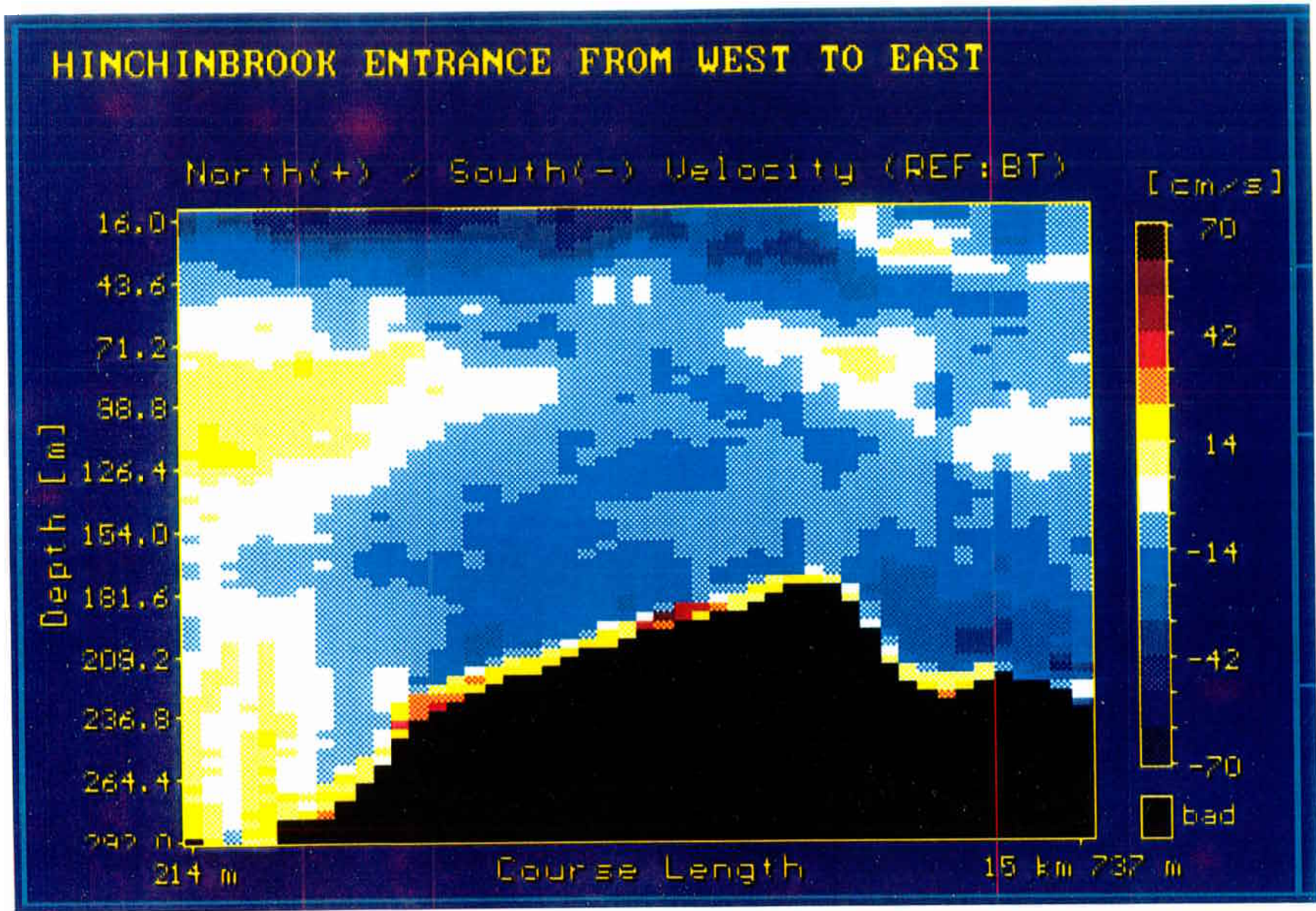
Figure 12b) ADCP velocities in Hinchinbrook Entrance. Salmon et al. data not to be published or cited elsewhere without written permission.

We present here a summary and some figures from a data report on regional hydrography of embayments in western PWS. The figures are illustrative of the types of analyses we have undertaken so far in examining the smaller scale hydrography of regions in western PWS.

Hydrography of Embayments in Western and Southwestern Prince William Sound, Alaska during Spring and Summer of 1994

Summary

Temperature and salinity (T/S) observations were made from May 18 to July 17, 1994 for various bays, inlets and fjords located in PWS. Basins surveyed included small, shallow to moderately deep bays and inlets, large deep bays and fjords, and small passes, located within five subregions: 1) West Knight Island; 2) South Ester, Perry and Culross Islands; 3) the mainland from Port Nelly Juan to Dangerous Passage; 4) Whale Bay to North Evans Island; and 5) Lower Prince of Wales Pass (PWP) and North Elrington Pass. Most bays were open at their mouths to the larger passes, except five locations which were either partially or totally silled.

Bays surveyed in May generally showed weak thermal stratification and the lowest variation in T/S properties. Regional patterns in T/S profiles were evident in May, and became more distinct as summer progressed. By June, all locations exhibited substantial thermal stratification as temperatures increased within the upper 15 m. Steeper gradients in near surface salinities also appeared as fresh water, principally from runoff, began to mix through surface layers.

The extent of surface freshening in June varied considerably between regions, and to a lesser extent, between bays within regions, corresponding with differences in local hydrology. The bays at West Knight Island exhibited the lowest changes in surface salinities, decreasing on average by less than 2 psu, whereas the bays located on the mainland displayed substantial decreases in surface salinities of up to 7 psu. The locations at South Perry Island were intermediate in variability of salinities, with average decreases of about 4 psu.

Thermal stratification continued into July at all locations resurveyed from June, with vertical temperature gradients ranging from -0.25 to -0.6 °C/m over depths of 3 to 20 m and 1 to 10 m respectively. The fjords at West Knight Island exhibited the highest range of surface temperatures (13.2 to 14.5 °C) with vertical gradients of about -0.4 °C/m, whereas Whale Bay (Region IV) displayed the steepest gradient (-0.6 °C/m.) with a slightly lower average surface temperature (12.6 °C). Locations surveyed in July within Lower Prince of Wales Pass were exceptional in that they exhibited very limited development of vertical temperature gradients (-0.09 °C/m.). T/S profiles for this area generally resembled profiles observed in May within other regions, the difference being slightly greater ranges in temperature at Lower PWP. This indicated that frequent vertical mixing was occurring in the extreme southwestern portions of PWS, probably resulting from tidal mixing and interactions with the Alaska Coastal Current. Two bays located on the southwestern side of Knight Island (Region I), Mummy Bay and Little

Bay, also exhibited more uniform T/S profiles in July, possibly due to similar factors.

Depths of isohalines varied considerably from May to June due to buoyancy changes resulting from heat and fresh water inputs. The locations at South Perry Island (Region II) and on the mainland (Region III) received large amounts of fresh water during this period and therefore, exhibited substantial depressions of the upper depth isohalines (27 to 30 psu) by up to 10 m. However, at most locations resurveyed in June there was a general upward movement of deeper isohalines (31 to 32 psu) by as much as 10 to 20 m. This pattern continued into July for the fjords and inlets in Region I, and also for most locations within Region IV (Whale Bay, Bainbridge Pass and Flemming Island).

In certain bays without sills, a significant upward displacement of very deep isohalines (>80 m.) occurred between June and July in conjunction with slight increases in heat ($\Delta T = + 0.5$ to $0.75°C$) and salinity (> 32 psu) at depths below 90 to 100 m. The deep temperature minima associated with this phenomenon appeared on T/S plots for entire basins, but the actual changes occurred only at stations located near the mouths of bays and inlets. Similar changes in T/S characteristics were observed at stations located in the passes adjacent to the bays, as deep water renewal occurred in bays to replace surface outflow into the passes, an example of classic estuarine circulation.

Locations exhibiting varying degrees of deep water replacement in conjunction with increased surface freshening included the following: Region I) Herring Bay and Long Channel; Region II) South Bay and Southeast Perry Island; Region III) Main Bay (changes occurring just outside the sills, but not inside the bay); Region IV) Whale Bay, Bainbridge Pass and Flemming Island; and Region V) Sawmill Bay possibly. Bays with sills and other obstructions at their mouths displayed decreased stratification at depths below 20 m, but no appearance at depth of water of higher salinity and temperature. This pattern was consistent during all months and reflects tidal mixing occurring in the lower portions of these bays, caused by the obstructions at their entrances. Such locations included Lower Herring Bay, Drier Bay, Culross Bay, and Main Bay. Other observations of mixing caused by restricted tidal flow occurred in deep passes where either sills or narrows exist, such as Bainbridge Pass, Upper Prince of Wales Pass, and Northwest Knight Island Pass. These phenomena appeared as tide rips at the surface with flotsam lines parallelling upwelling zones.

We include here a few figures that exemplify property distributions and phenomena discussed in the above summary.
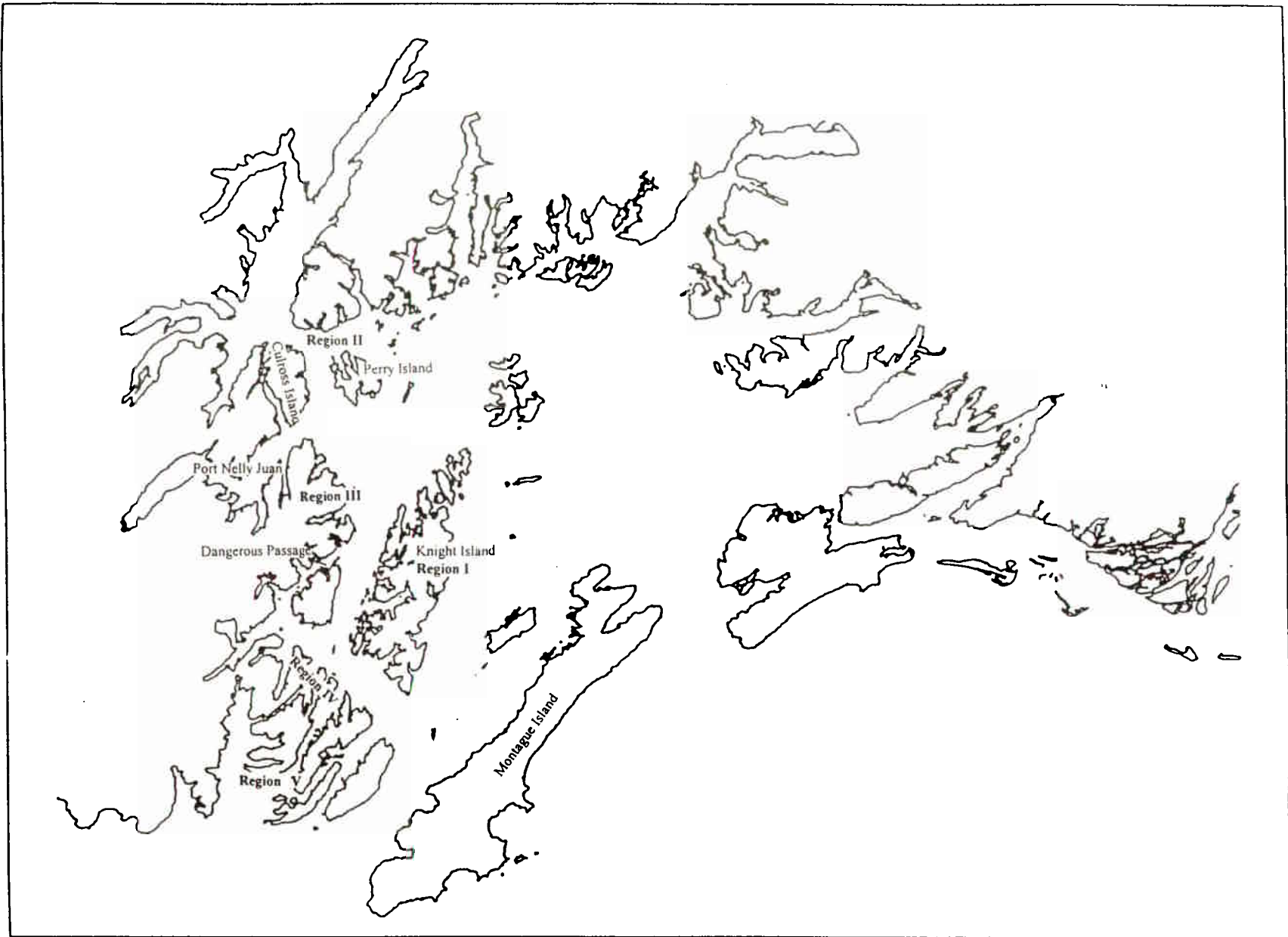
Fig. 1. Map of Prince William Sound, Alaska and Regions of Embayments Surveyed in 1994.
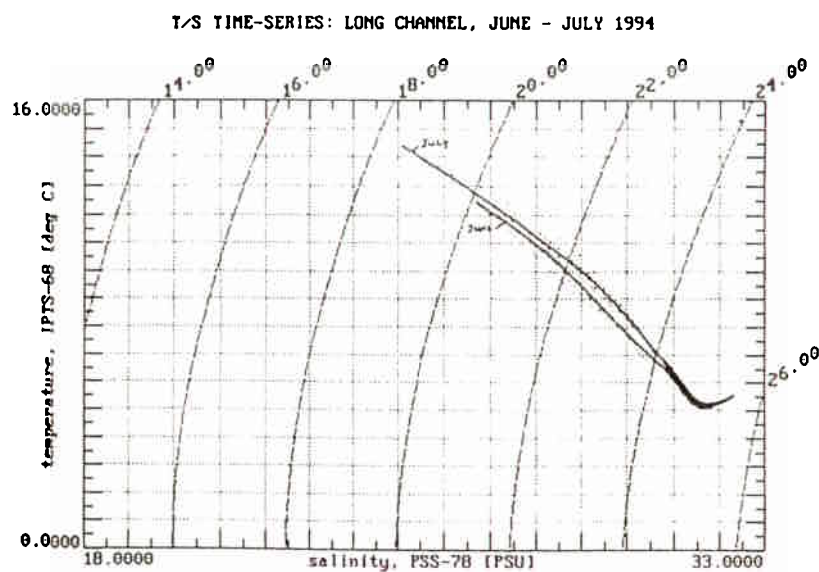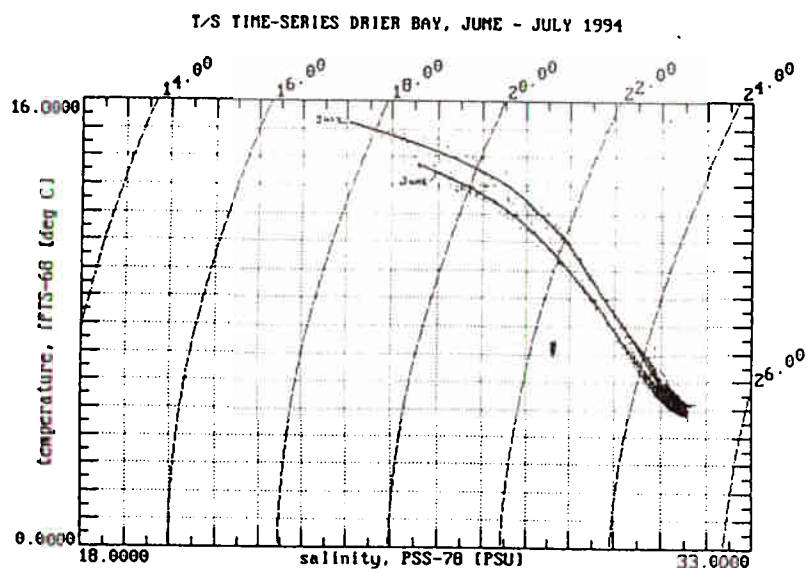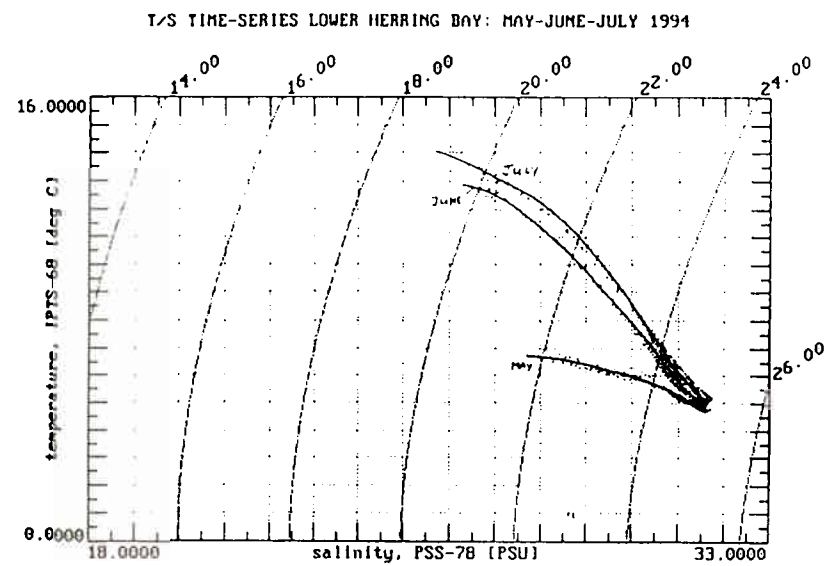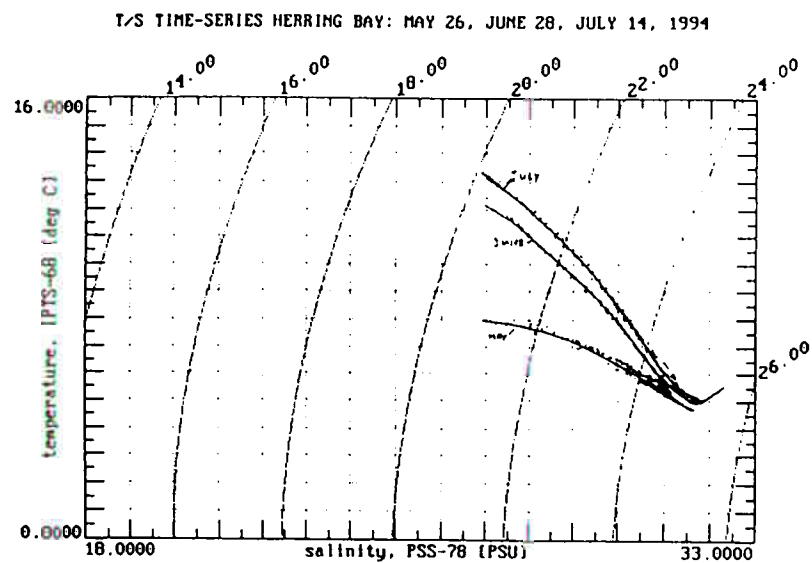
Fig. 3.   Temperature vrs. Salinity Time-Series. May to July, 1994: a) Herring Bay, b) Lower Herring Bay.
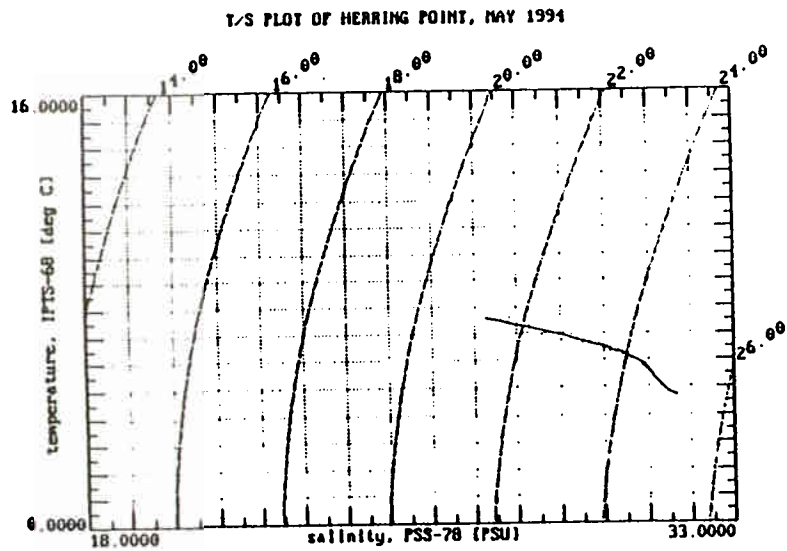June to July, 1994: c) Drier Bay, d) Long Channel.

T/S PLOT OF HERRING POINT, MAY 1994

T/S PLOT OF AGULIAK ISLAND, JULY 1994

T/S PLOT OF MUMMY BAY (S. KNIGHT ISL.), JULY 1994

T/S PLOT OF LITTLE BAY (S. KNIGHT ISL.), JULY 1994
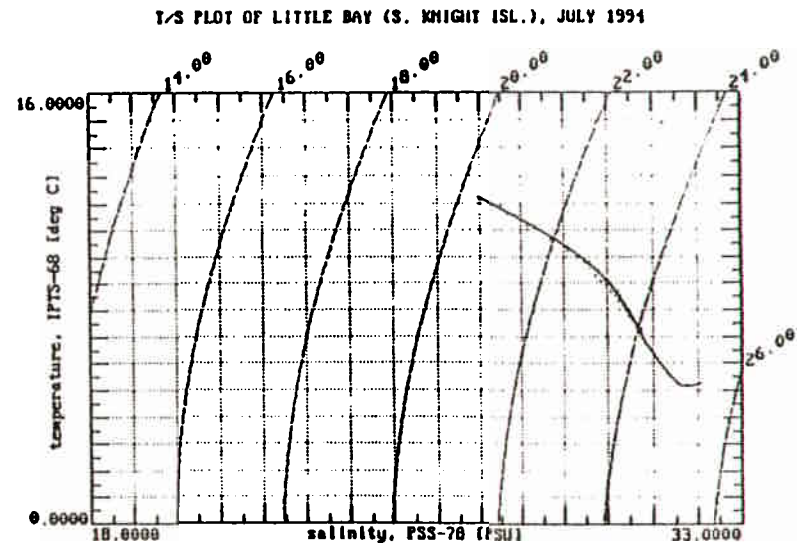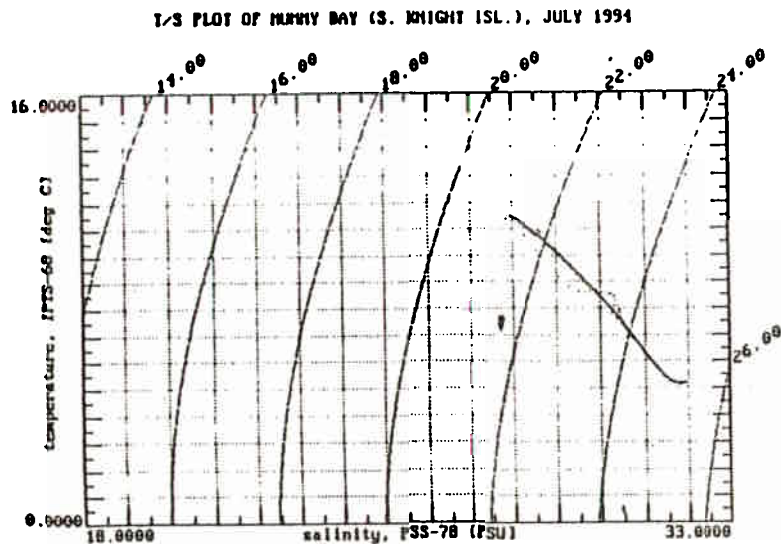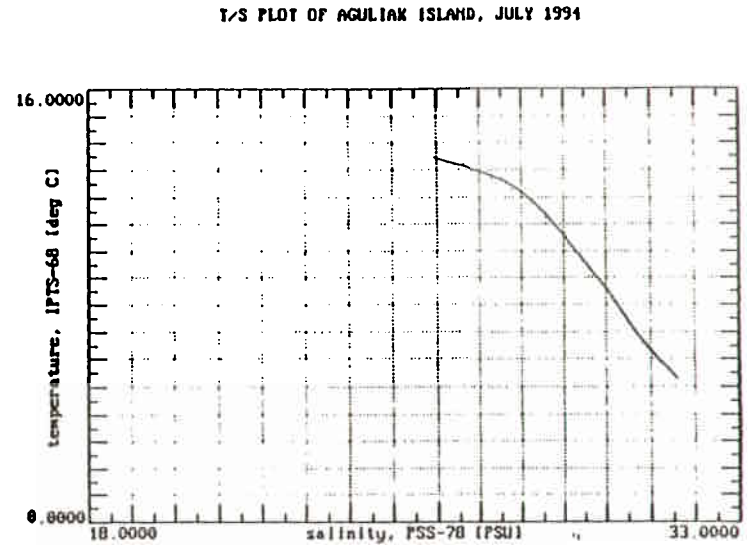
Fig. 3 (Continued).   May 1994: e) Herring Point. July 1994: f) Aguliak Island, g) Mummy Bay, h) Little Bay.
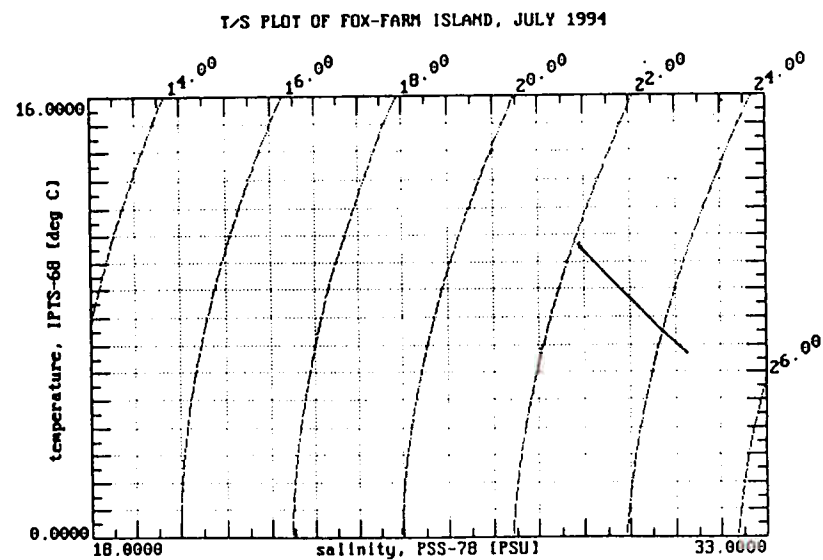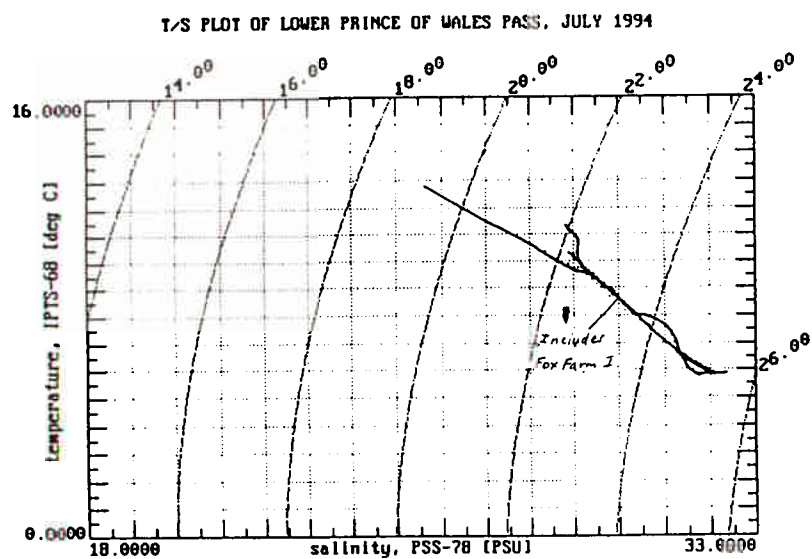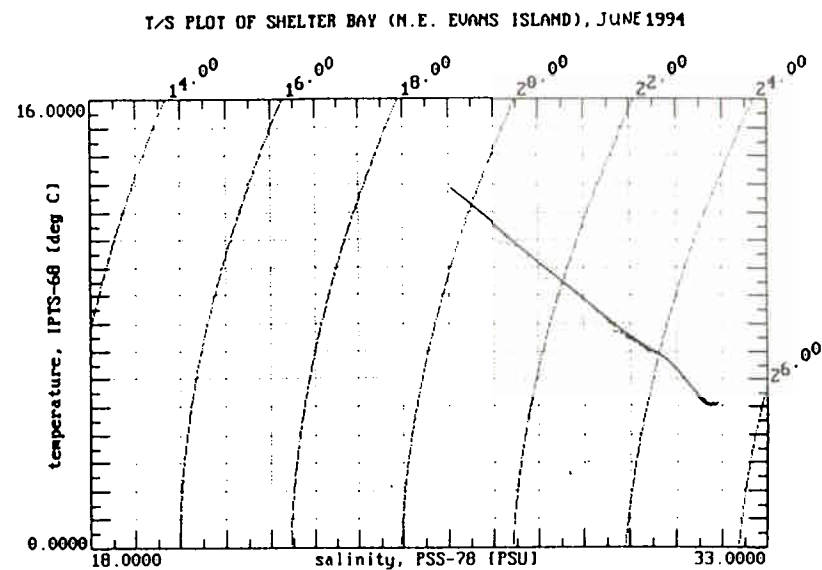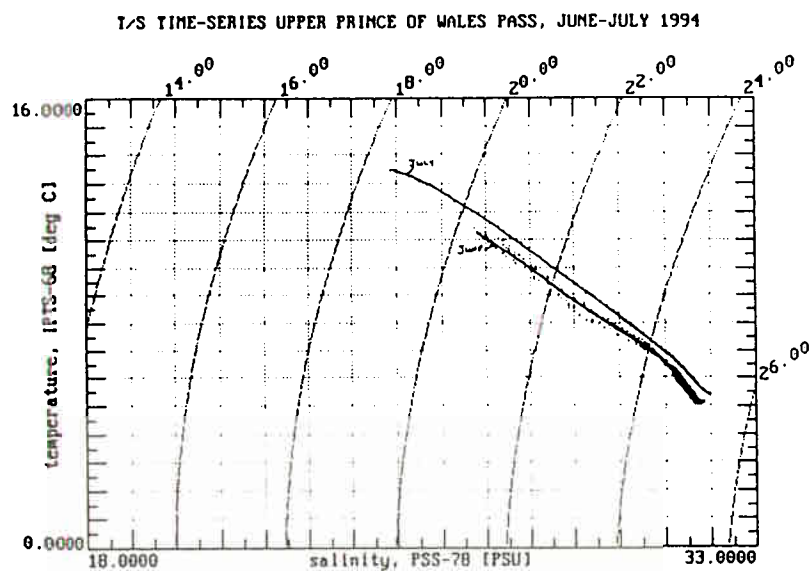
Fig. 27 (Continued). Temperature vrs. Salinity Plots, June to July 1994. e) Upper Prince of Wales Pass, June to July 1994, f) Shelter Bay, June 1994, g) Lower Prince of Wales Pass, July 1994 , h) Fox Farm Island.
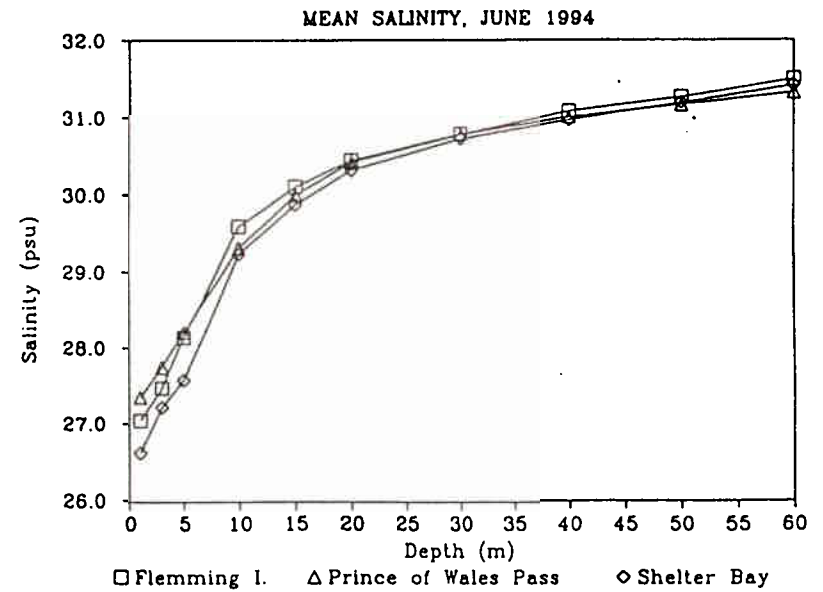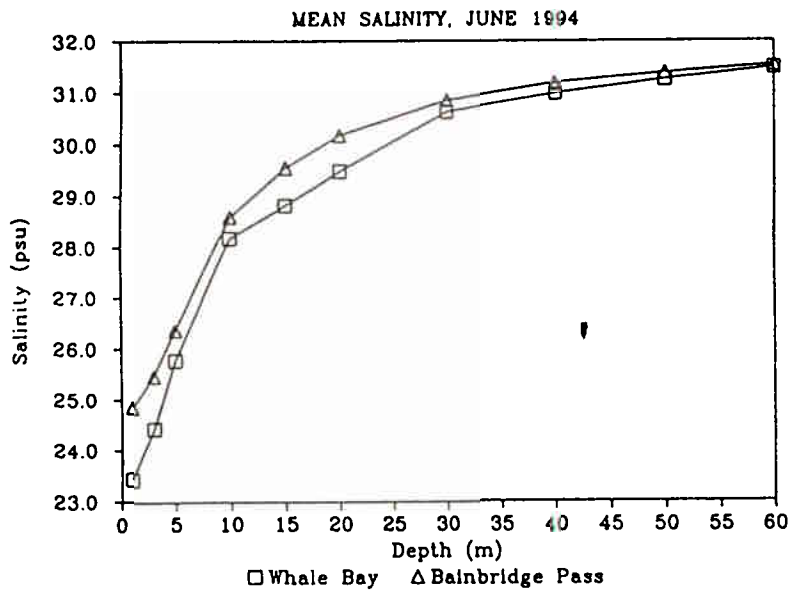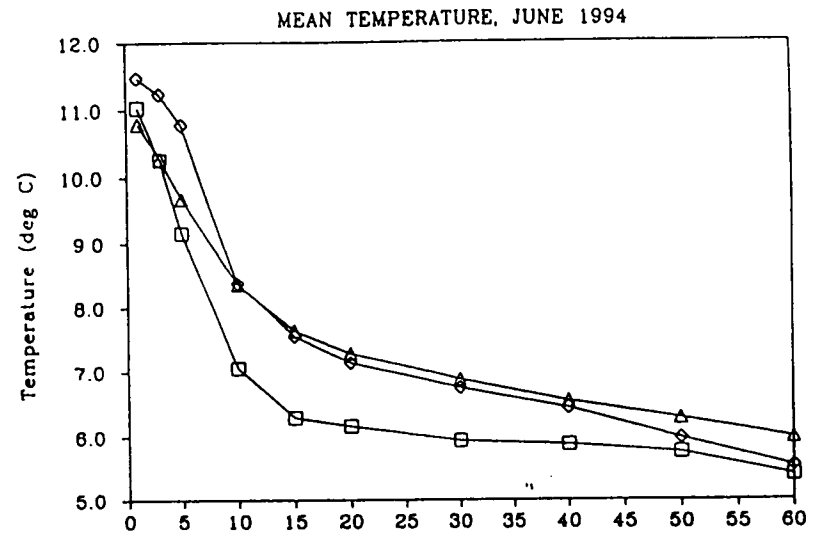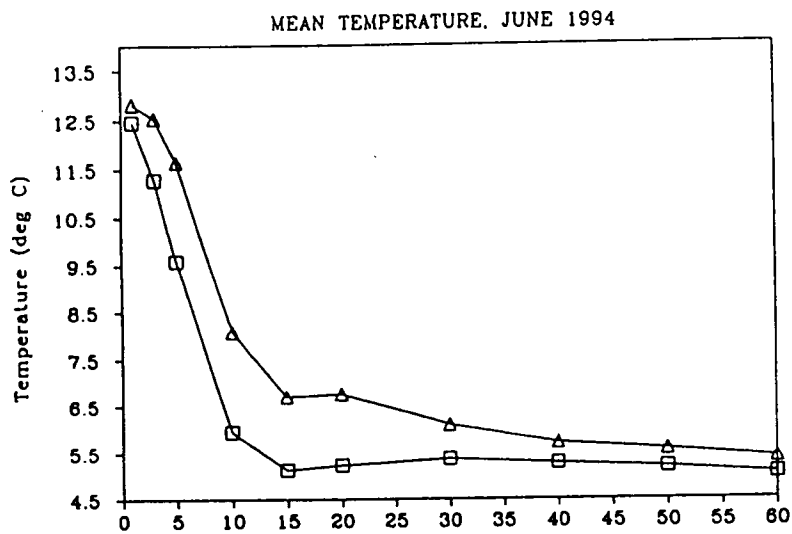
Fig. 28. Mean Temperature and Salinity from 1 to 60 m., June 1994. Whale Bay and Bainbridge Pass: a) Temperature, b) salinity. Flemming I., Prince of Wales Pass and Shelter Bay: c) Temperature, d) Salinity.
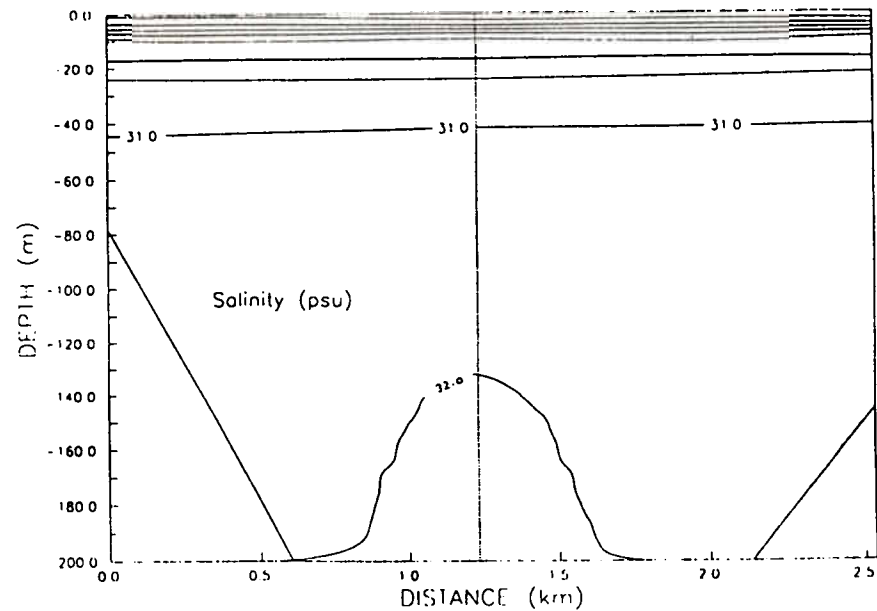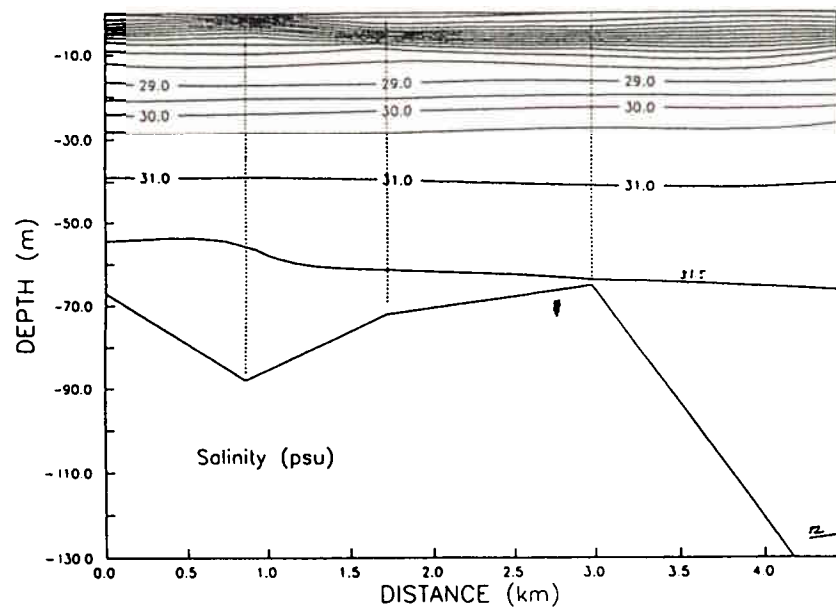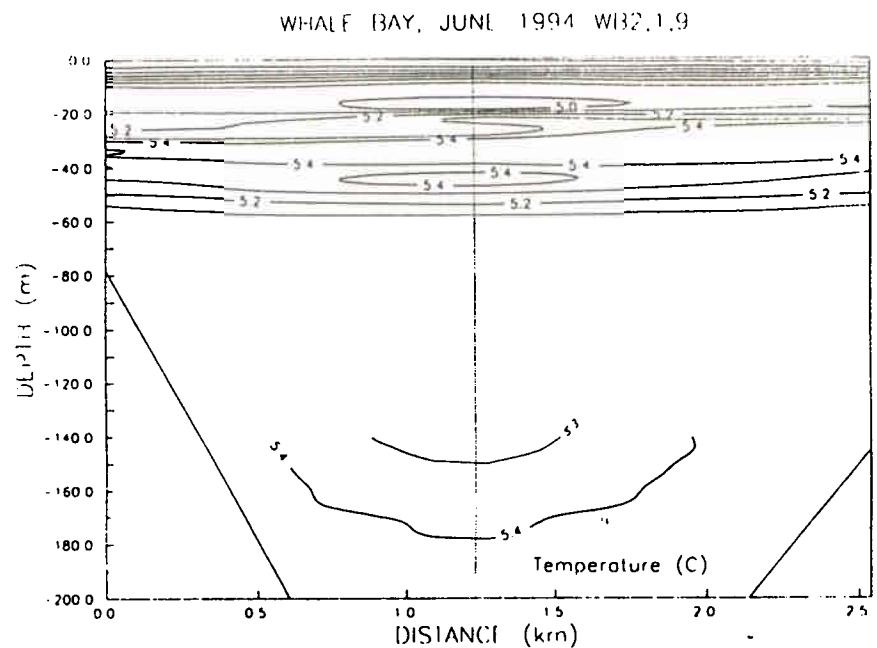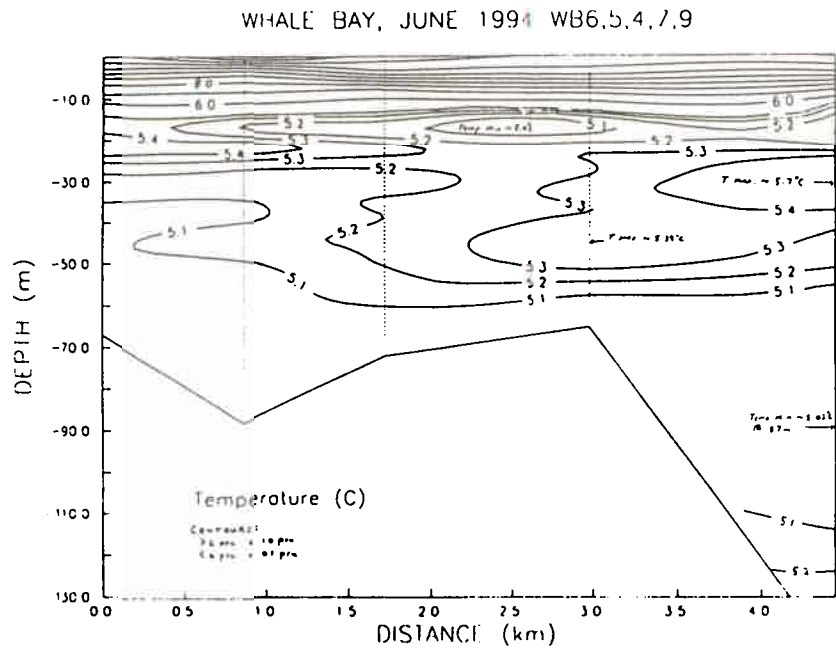
Fig. 29. Contours of Temperature and Salinity for Whale Bay, June 1994.   a-b) Stations WB6, 5, 4, 7 and 9.
c-d) Stations WB2, 1 and 9.
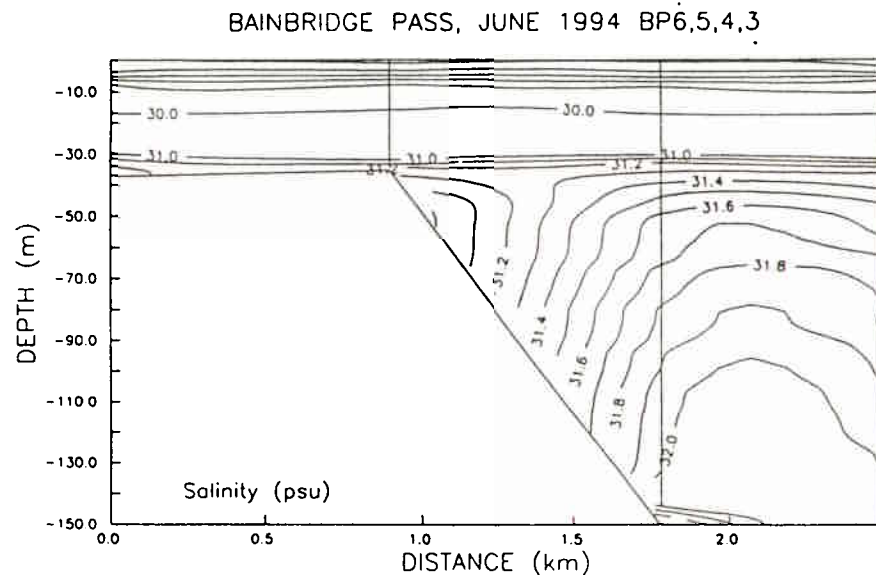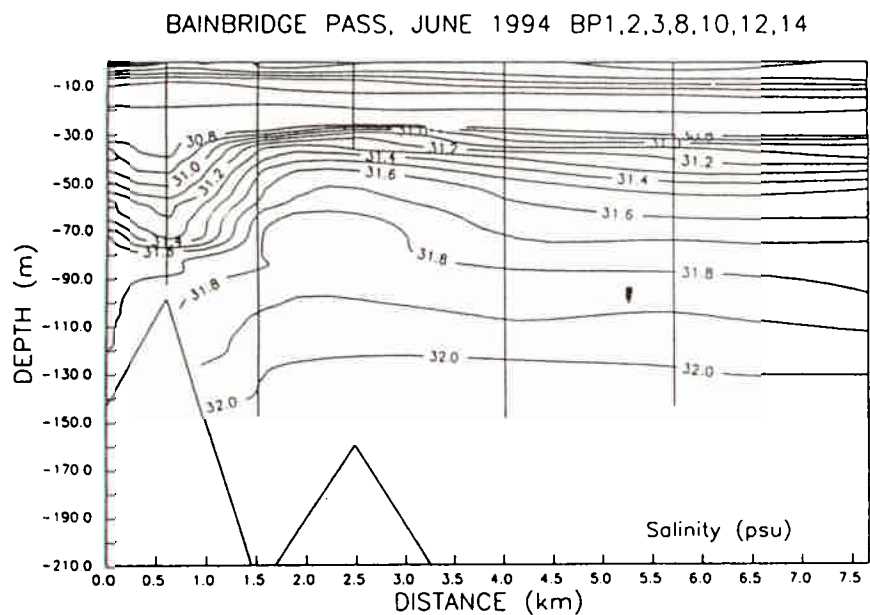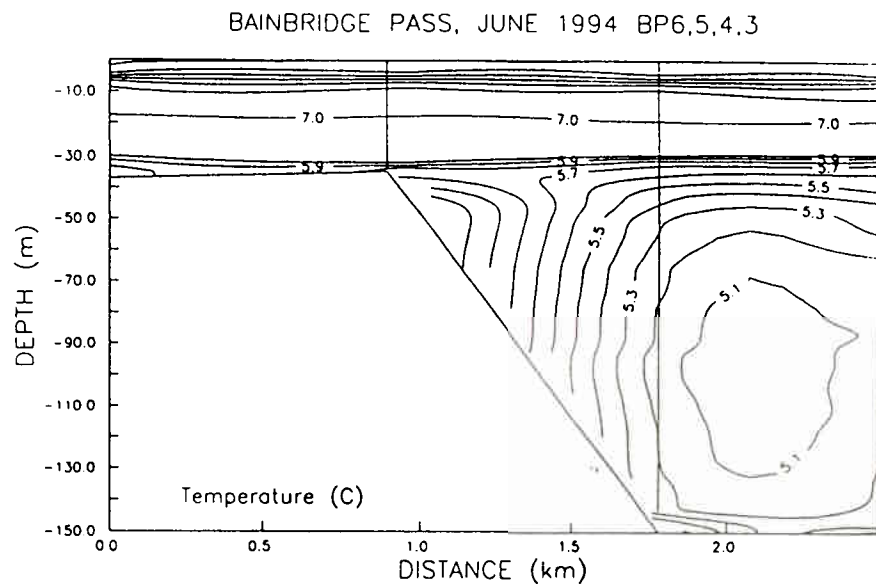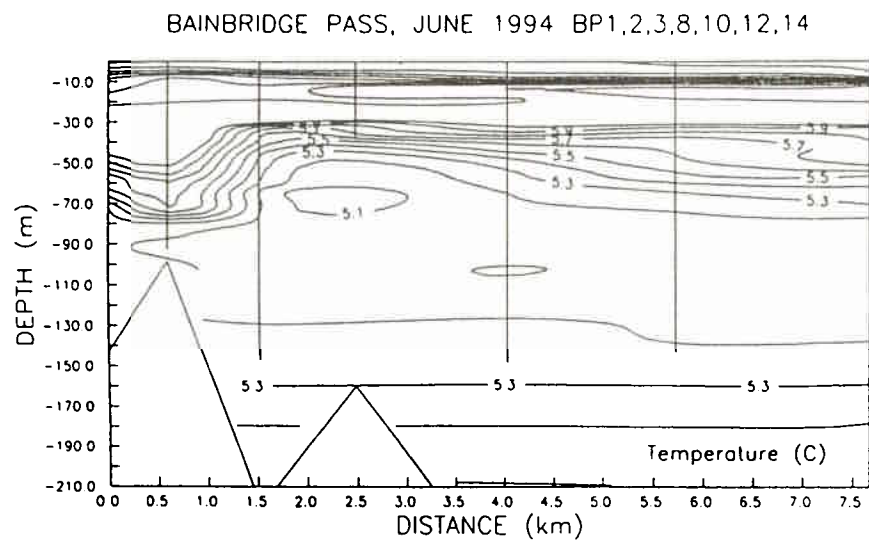
Fig. 30. Contours of Temperature and Salinity for Bainbr[...] Pass, June 1994. a-b) Stations BP1, 2, 3, 8, 10, 12 and 14. b-c) Station BP6, 5, 4 and 3.
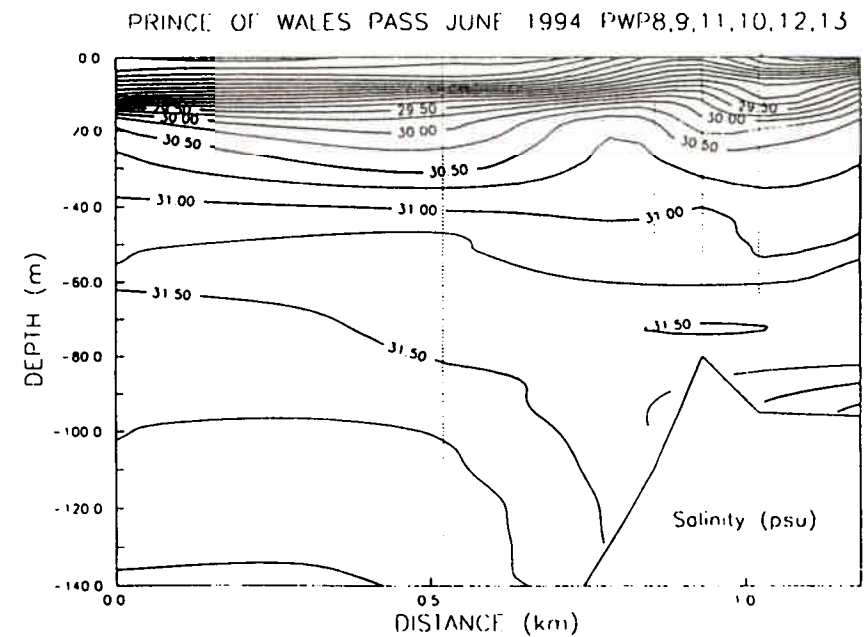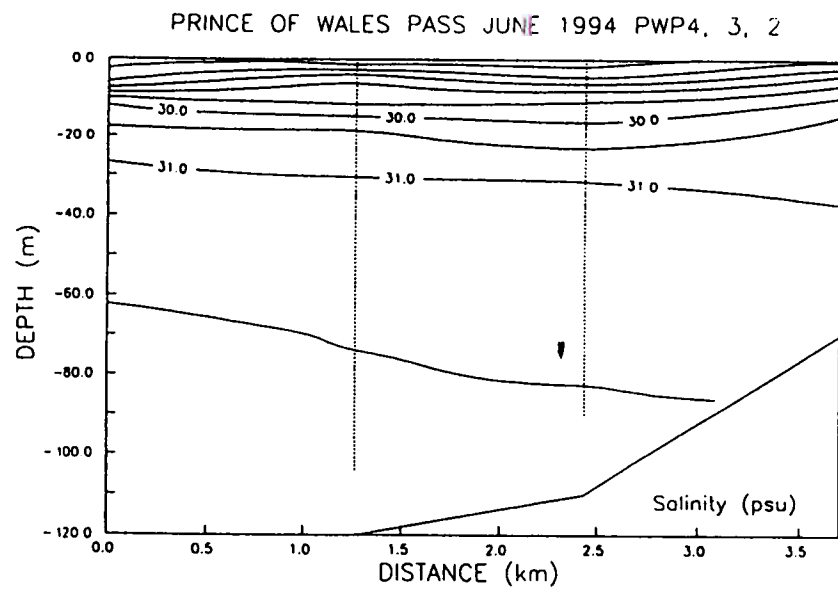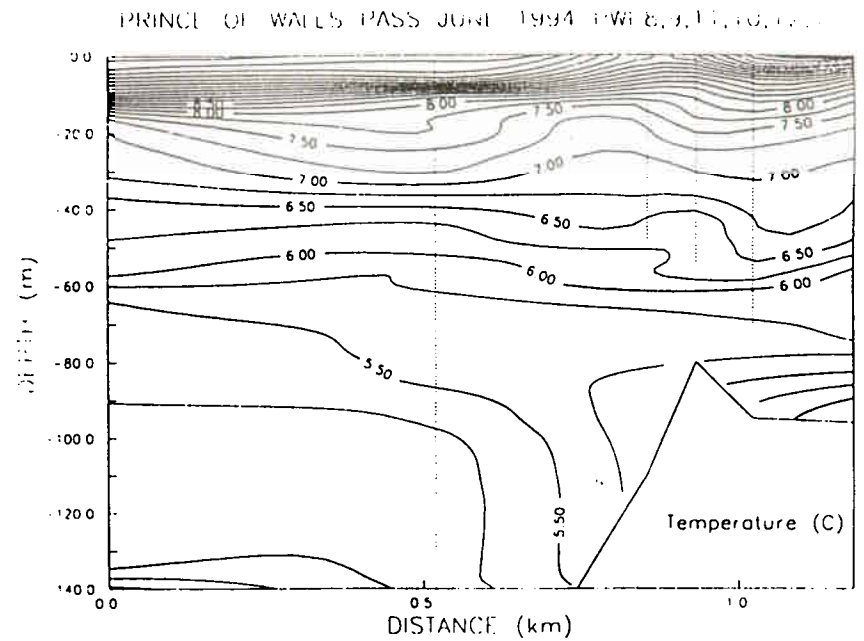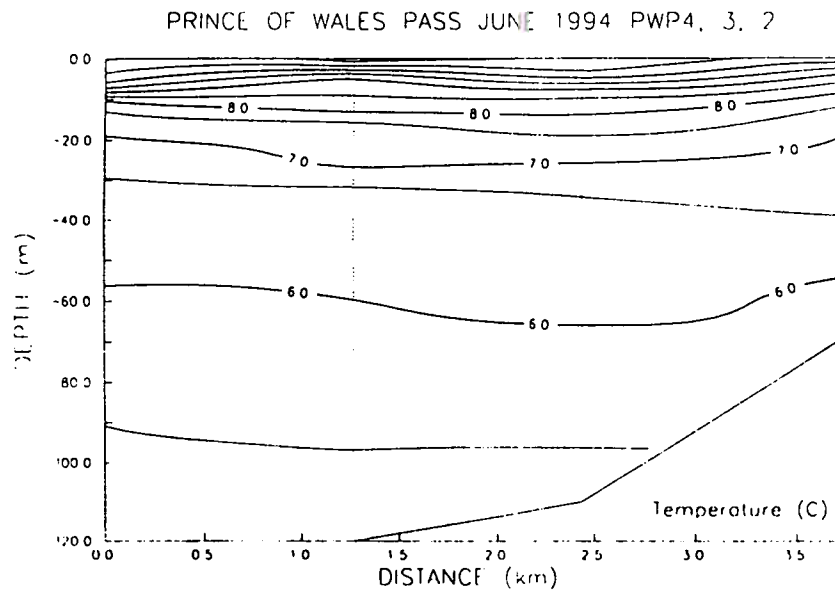
Fig. 31. Contours of Temperature and Salinity for Prince of Wales Pass, June 1994. a-b) Stations PWP4, 3 and 2.
c-d) Stations PWP8, 9, 11, 10, 12 and 13.